Newfound Intelligent Solution for Grid Connected PV Systems Diagnosis Based on CANFIS Algorithm

Chérifa Kara Mostefa Khelil[1, 3], Badia Amrouche[2, 3], Mohamed Nadjib BenAllal[1], Kamel Kara[3], Aissa Chouder[4].

[1,3]Electrical Engineering Department, Khemis Miliana University, Ain Defla (Algeria).

[2]Renewable Energies Department, Blida 1 University, BP 270 Blida (Algeria).

[3]SET Laboratory, Electronics Department, Blida 1 University, BP 270 Blida (Algeria).

[4]Electrical Engineering Laboratory (LGE), University Mohamed Boudiaf of M'sila, BP 166, 28000 (Algeria).

The Author's Email: k.karamostapha@univ-dbkm.dz[1], amrouche_badia@yahoo.fr[2], m.benallal@univ-dbkm.dz[3], km_kara@yahoo.fr[4], aissachouder@gmail.com[5].

Received: 07/2023 **Published: 08/2023**

Abstract:

The present article proposes a novel hybrid intelligent diagnosis solution for grid connected PV installations based on Co Active Neuro Inference System (CANFIS) algorithm. The considered faults are open circuit fault, short circuit fault, ground fault and by-pass diodes fault in PV array. This solution has been tested and validated on a 9.54 kWp grid connected PV installation. The performances of the proposed method has been tested by residual criteria citing: Mean square error (MSE), Root mean square error (RMSE), Mean absolute percentage error (MAPE), Mean absolute deviation (MAD) and coefficient of correlation (R^2) which display 4.65 % and 0.99. The isolation process has been performed using the percentage linear scatter plot of both electrical data (Impp, Vmpp) in the goal to obtain the global diagnosis of PV system. The main novelty of this work is the fact that the proposed diagnosis solution takes into account a particular class of faults which has been until now discarded because of the difficulty of its isolation ; these are faults linked to the bypass diode.

Keywords: Grid connected PV systems, faults classification, faults diagnosis, Artificial Intelligence, CANFIS algorithm.

Tob Regul Sci.™ 2023;9(1): 3809-3844

DOI: doi.org/10.18001/TRS.9.268

1. Introduction

At the present time, the diagnosis of photovoltaic systems is the current topic that allows to maintain performance from the point of view of the PV arrays' lifetime as well as to minimize human interventions with all that

this generates time. This topic is very intervening for several works with different methods, the interested readers will be able to refer to [1, 40].

In the precedent works relative to [20-22], the diagnosis of PV systems was based on different types of ANNs, where the results were successfully proven for open circuit fault as well as short circuit faults in PV array. In the perspective of the present work, the process has been enlarged by the adding of ground fault in addition to by-pass diodes fault in PV array that the researchers have found difficulties to treat it. Table 1 below represents computational intelligence for PV system diagnosis mentioned with meticulous details from point of view of advantages and drawbacks for different references.

Table 1

Advantages and limitations of PV systems' fault diagnosis (Kara Mostefa Khelil et al., 2022).

References	Intelligent methods	Advantages	Limitations
(Hussain et al., 2020)	• MLP	Only two parameters are used in fault detection (Irradiance and PV output power). The best accuracy is from the MLP containing 3 hidden layers equals to 99.1%. Four different methodologies of ANNs have been used with different architectures.	In presence of shading case the accuracy decreases to 96.2%
(Garoudja et al., 2017)	• ANN • PNN	Comparative study between ANN and PNN in term of diagnosis of PV system. Can diagnose many faults in presence of noise. Excellent level of accuracy with 100%.	Four parameters (PV temperature, solar irradiation, Impp, Vmpp) in the same intelligent bloc. Not able to diagnose by-pass diode faults.
(Kara Mostefa Khelil et al., 2020)	• ANNs	Two ANNs are used in conjunction with a combinational logic block. Based on experimental testing conditions, the diagnosis success rate is 98.6%. Simplicity and rapidity for both detection and localization.	Neglected confusion in current and voltage classification.
(Kara Mostefa Khelil et al., 2021)	• MLP • RBFNN	The impact of the ANNs' choice on PV systems diagnosis quality is addressed.	Very careless misclassification voltage.

	• PNN GRNN	The efficiency of an ANNs based intelligent diagnosis algorithm is analysed. Five ANNs are considered: BPNN, Two RBF, PNN and GRNN. The comparison takes into account the accuracy, the specificity, the sensitivity and the rapidity. Response time of each algorithm has been taken in consideration. The results identify the PNN as the best candidate for the studied diagnosis task with 100% in all key statistical concept and the fastest in response time.	
(Kara Mostefa Khelil et al., 2022)	• Bayesian NN	Two climatic parameters and two electrical parameters have been used Short response time diagnosis Excellent accuracy with 99.88%	Some samples in misclassification between two PV modules short circuited and one PV module short circuit.
(Li et al., 2021)	• ANN	Reach demonstration with documentation about Fault detection and diagnosis of PV systems. Statistical concept in fault detection in PV systems using different type of AI especially various cases of ANN.	Doesn't take in consideration the response time for each kind of these methods.
(Madeti et al., 2018)	• KNN	High accuracy of 98.70%. Operates in online fault. Less computational time.	Confusion classification between: ✓ Open circuit and shading with bypass diode normal. ✓ Line-line and shading with inverted bypass diode. ✓ Shading with faulted bypass diode and shading with bypass diode normal.

(Dhimish et al., 2018)	• ANN • Fuzzy Logic	Developed and comparative study between ANN and Fuzzy Logic (Mamdani and Sugeno). Two attributes as input data (voltage and Power) Ratio. Easy and fast for both machine learning in fault detection of PV systems. High detection accuracy especially for ANN.	Fuzzy logic method requires a lot of mathematical expressions.
(Dhimish et al., 2017)	• Fuzzy Logic	Capability to detect hot spot in PV system in addition to faulty PV modules using Fuzzy Logic. Minimum detection accuracy equals to 98.8% and maximum equals to 99.31%. Easy to use in fault detection and diagnosis of PV systems. The algorithm can be used with wide range of PV installation.	The accuracy of the algorithm depends on the instrumentation used in the PV plants. Not able to detect fault occurring in the bypass diode.
(Chine et al., 2016)	• ANN	Two algorithms have been used: The first has been consecrated for the implementation of a signal threshold approach. The second consists of an ANN-based approach. Ability to localize and correctly identify the different faults with neglected confusion.	The approach used only the electrical attributes as input data (Impp, Vmpp, Voc, Isc).
(Liao et al., 2017)	• PSO	High Accuracy in fault detection of PV systems with PSO equals to 93.33% . Different cases of faults diagnosis including in some cases two failures in the same fault (eg: the combination of temperature fault and aging cells). Can predict the fault type in real time without additional hardware support.	The approach used only the electrical attributes as input data (Voc, Isc , Pmpp, Vmpp). The response time was not mentioned for both intelligent methods.

			No indication about the confusion classification between classes.
(Belaout et al., 2018)	• ANFIS • MLP	The fault detection is based on threshold between healthy and faulty PVA. Multiclass classification employing different MFs Comparative study between neuro-fuzzy classifier and MLP. Precision is 99.15%.	12 features have been used to ensure the detection of global PVA.

The remainder of this article is organized into four parts. Section 2 exposes the Co Active Neuro Inference System (CANFIS), Section 3 gives the presentation of experimental PV setup. Section 4 represents methodology, Section 5 presents the results and their discussion. At the end, the conclusions and recommendations are set out in Section 6.

2. Hybrid Neuro-Fuzzy developed algorithm (ANFIS)

Adaptive Neuro Fuzzy Inference system or Neuro Fuzzy logic is a Hybrid Artificial Intelligence system according to the literature is called Neuro Fuzzy System (NFS) or Fuzzy Neural Network (FNN) [41]. This type of hybrid artificial intelligence is considered as a powerful tool from point of view of its clear interpretation of the output results as well as simple extension of the ability by the insertion of the new rules. This ANFISs issue from combination between artificial Neural Network that are responsible to represent the structures and Fuzzy logic by the employment of the fuzzy production rules and membership functions that are automatically achieved as well as adjusted from the pick-up numerical data employing if- then rules that give authorization to obtain an extra robust model [42]. Control designates the main aspect of ANFIS applications for the reason that in this case the research focuses on the approximation of nonlinear functions, particularly in the modeling and identification classes of systems [43]. Habitually, the Takagi–Sugeno fuzzy inference system is frequently used for its precision model, where a fuzzy rule has a role to combine the crisp linear inputs rather than a fuzzy set. A classical rule set using two fuzzy IF-THEN rules in the first order of Takagi–Sugeno fuzzy inference model can be demonstrated as:

- C1 is calculated by the rule below:

$$IF\ (T\ is\ A1)\ AND\ (G\ is\ B1)\ THEN\ (C1 = P_1T + Q_1G + r_1) \quad (1)$$

- C2 is calculated by the rule below:

$$IF\ (T\ is\ A2)\ AND\ (G\ is\ B2)\ THEN\ (C2 = P_2T + Q_2G + r_2) \quad (2)$$

Here A_1, A_2 and B_1, B_2 are membership values with C_1 and C_2 of input variables T and G, respectively. P_1, Q_1, r_1 and P_2, Q_2, r_2 are the parameters are obtained during the training process. ANFIS can adjust these fuzzy (If-Then)

rules and membership functions in the goal to reduce the output error measure or to clarify the relationship between the input– output for complex systems [44].

2.1. CANFIS algorithm architecture

The Co Active Inference System model belongs to the ANFIS model. we can consider that it is a globalization of ANFIS with the conservation of all the advantages of its precedent reflecting on a global approximation of the general nonlinear function. The main objective of the CANFIS model is to solve one of the critical weaknesses of ANFIS systems while maintaining the fundamental rules [42]. From an architectural point of view, the source of the powerful capability of CANFIS comes from the model-dependent weights between the consequent layer and the fuzzy summation layer [45]. Typically, in this type ANFIS of general bell-shaped, Gaussian and sigmoidal (MF) membership functions (MFs) have been introduced by a fuzzy control system. A basic reasoning of the Takagi–Sugeno inference system produces an output function f from the input variables T and G are shown in Fig. 1 which represents the CANFIS structure, where the above rules are implemented. In this figure, the squares indicate the adaptive nodes, while the circles represent the fixed node. Five main layers make up the CANFIS model and each layer performs a specific task in the FIS (Fuzzy Inference System) demonstrated as follows:

Layer 1 (Premise layer): Each adaptive N node in this layer is labeled by square and represents a node function, demonstrated as follow:

$$O_{i,1} = \mu_{Ai}(T) \qquad i = 1,2 \qquad (3)$$

$$O_{i,1} = \mu_{Bi-2}(G) \qquad i = 1,2 \qquad (4)$$

Where T, G are the input to node i, and A_i, B_{i-2} are the linguistic label (small, large, etc.) denoted by favorable membership functions (MF's) $\mu_{Ai}(T)$ and $\mu_{Bi-2}(G)$. Generally, in the CANFIS model, the MF's can take some functions such as: Gaussian, sigmoid or bell-shaped where their equations is demonstrated in Table 2.

Table 2

The basic MF's used in the study.

MFs' Names	Equations
Gaussian	$\mu_{Ai}(T) = e^{-\frac{(T-c)^2}{2\sigma^2}}$ (5)
Sigmoid	$\mu_{Ai}(T) = \frac{1}{1+e^{-a(T-c)}}$ (6)
Bell-shaped	$\mu_{Ai}(T) = \frac{1}{1+\left\|\frac{T-c}{a}\right\|^{2b}}$ (7)

The same thing can be used with $\mu_{Bi-2}(G)$ and replace T by G. where the a, b, c, σ are the parameters that change the shapes of the MFs over an interval of]0, 1[[46].

Layer 2 (Product layer): In this layer, the nodes represented in the circles labeled by ∏ apply the rule operator (AND / OR) in order to provide one output which indicates the antecedent's results for a fuzzy rule that multiplies the entering signals, as follow:

$$O_{i,2} = w_i = \mu_{Ai}(T) * \mu_{Bi}(G), \qquad i = 1,2 \qquad (8)$$

Here $O_{i,2}$ is the output of the layer 2, and the output signal w_i indicates the firing strength of the rule.

Layer 3 (The rule or Normalization layer): Is non-adaptive layer, where the nodes represented in the circles are labeled by N then they compute the ratio of the firing strength of the ith rule to the sum of the firing strengths of global rules as follow:

$$O_{i,3} = \overline{w} = \frac{w_i}{w_1+w_2}, \qquad i = 1,2 \qquad (9)$$

The outputs of this layer ($\overline{w}$) is known as normalized weights or normalized firing strengths (Quej et al., 2017).

Layer 4 (Defuzzification or Consequent layer): In this layer the nodes are symbolized by squares, where each linear function computed the weighted output as follow:

$$O_{4,i} = \overline{w_i}C_i = \overline{w_i}(P_iT + Q_iG + r_i), \qquad i = 1,2 \qquad (10)$$

Here, $\overline{w}$ is the output of layer 3; P_i, Q_i and r_i are considered as consequent parameters of a linear combination in the Sugeno inference system.

Layer 5 (Output or Fuzzy association layer): The role of this layer is to combine the total inputs coming from the consequence layer, then transforms the fuzzy classification outcomes into an original output. In this layer, the node is non adaptive and calculates the global output of total incoming signals as follow:

$$O_{5,i} = \sum_i \overline{w_i}C_i = \frac{\sum_i w_i C_i}{\sum_i w_i} = f\ out = estimated\ global\ output,\ i = 1,2 \qquad (11)$$

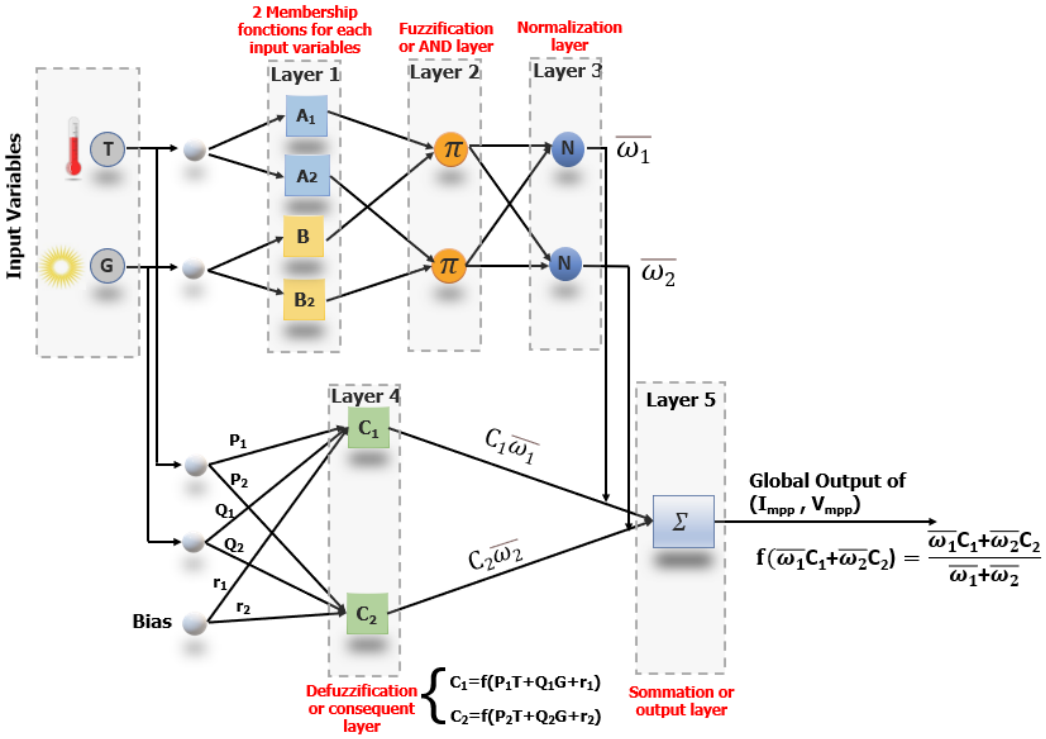

Fig. 1. CANFIS architecture.

2.2. Performance of the CANFIS model in GCPV systems

In order to evaluate the performance of the CANFIS algorithm in a grid-connected PV array compared to the real measured model, some residual criteria must be considered, such as: (MSE) the Mean Square Error, (RMSE) the Root Mean Squared Error, (MAD) the Mean Absolute Deviation, (MAPE) Mean Absolute Percent Error as well as

(R^2) Correlation Coefficient shown in equations (12, 13, 14, 15, 16) respectively, where y_n is the n^{th} measured datum, $\hat{y}_n$ is the n^{th} simulated data and N is the size of the database (the number of validation epochs) [20]. Be aware that the validation data of the performance evaluation stage are the inputs of the algorithm which are the operating conditions of the PV plan (the solar irradiation and the PV temperature), and the output data are the current and the voltage at MPP:

$$MSE = \frac{1}{N}\sum_{n=1}^{N}(y_n - \widehat{y_n}) \quad (12)$$

$$RMSE = \sqrt{\frac{1}{N}\sum_{n=1}^{N}(y_n - \widehat{y_n})} \quad (13)$$

$$MAD = \frac{1}{n}\sum_{n=1}^{N}|y_n - \widehat{y_n}| \quad (14)$$

$$MAPE = \frac{1}{n}\sum_{n=1}^{N}\frac{|y_n - \widehat{y_n}|}{|y_n|}x100\% \quad (15)$$

$$R^2 = 1 - \left(\frac{\sum_{n=1}^{N}(y_n - \widehat{y_n})^2}{\sum_{n=1}^{N}(y_n)^2}\right) \quad (16)$$

3. Presentation of experimental PV setup

According to the approaches cited in [20- 22], the fault diagnosis of small grid connected of a PV plan has been developed employing an intelligent algorithm founded upon different methods of ANNs, where the results were obtained with success. The PV array in this study is composed by thirty PV modules shared in two branches and each branch contains fifteen PV modules linked in series. The characteristics of the PV module as well as the electrical properties of the PV array used in this work are summarized in Table 3 and Table 4 respectively.

Table 3

Electrical properties of the Isofoton 106-12 PV module [20- 22].

Solar Panel electrical characteristics	Value
Peak power	106 W
Short circuit current (Isc)	6.54 A
Open circuit voltage (Voc)	21.6 V
Voltage at Maximum Power Point (Vmpp)	17.4 V
Current at Maximum Power Point (Impp)	6.10 A
Number of cells connected in Series	36
Number of cells connected in Parallel	2
Cell Short circuit current	3.27 A
Cell Open circuit Voltage	V

Table 4

Components and characteristics of PV installation [22].

Components	Characteristics
Global PV array	90 PV modules with monocrystalline technology
PV Sub array studied	30 PV modules divided in two strings : 15 x 15
Sunlight apparatus	Thermoelectric Pyranometer
Temperature apparatus	K-type thermocouple Pilot PV cell
Data logger	Agilent 34970A
Inverter	IG30 Fronius

4. Methodology

4.1. Data analysis

Class's Identification, localization, isolation and diagnosis are an inescapable trend with a view to guarantee the stability, efficiency, reliability in addition to the quality of the grid connected PV system. For this, the present approach is divided into three important steps:

- In order to test the accuracy of the CANFIS algorithm, the first step described in Fig. 2 is necessary requiring real climate data: Temperature (°C), Solar Irradiation (W/m2) in addition to electrical data: Current (Impp (A)) and voltage (Vmpp (V)) at maximum power point. The number of samples used in this approach is 5550 samples for each attribute cited above in this section (Temperature, solar irradiation, current and voltage at maximum power point) divided in 3000, 1250 and 1300 for training, checking and testing phases respectively. This stage is considered as comparative part employing residual criteria (MSE, RMSE, MAPE, MAD and R^2) between electrical data furnish from real PV array and two CANFIS blocs, each bloc is devoted to provide the predicted electrical data (Impp, Vmpp) separately from the same real climate data of PV array.

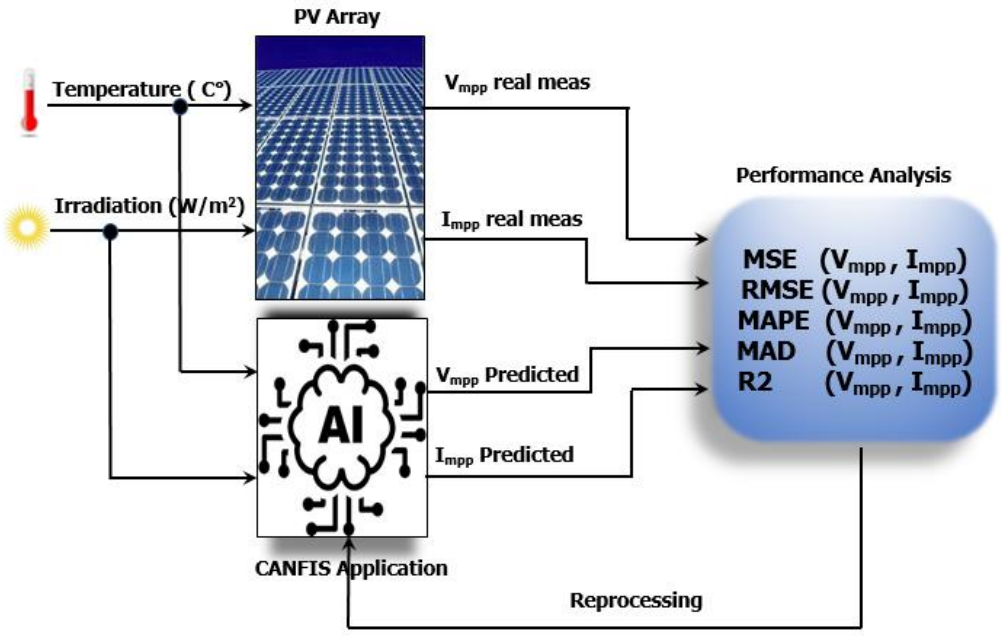

Fig. 2. Performance analysis scheme between real and predicted data of PV array.

- The second and the third steps are illustrated in the Fig. 3, the isolation and analyzation through the deviation propose in percentage (the scatter plot in linear percentage deviation) between real healthy electrical output data coming from PV array and predicted electrical output data issue from CANFIS algorithm of different faults covered in this work are depicted in second step.
- The third step represents the combination of the deviation of Impp and Vmpp of different class categories with the aim of obtaining the overall diagnosis of the designed PV system with a significant degree of accuracy and efficiency.

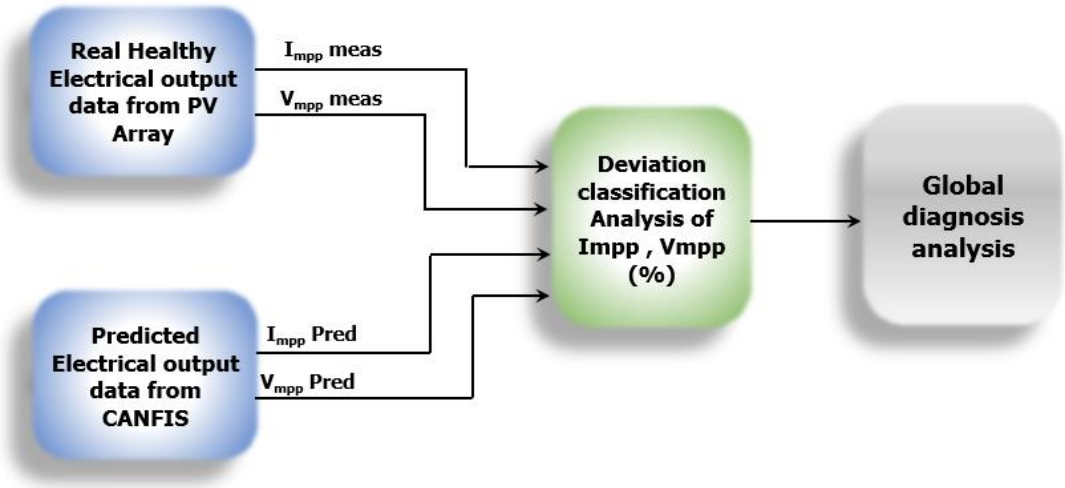

Fig. 3. Global diagnosis of PV array using percentage deviation process.

4.2. Fault detection and diagnosis procedure

The CANFIS algorithm is designed to analyze, identify and diagnose healthy case in addition to six faulty cases depicted in Fig. 4 (a, b) citing healthy case in (a) and in (b): 1) two PV modules short circuited in branch of PV array, 2) five PV modules short circuited in branch of PV array, 3) two inversed By-pass diodes, 4) ground fault and 5) open circuit branch in PV array. The Table 5 resumes all classes treated in this study over and above of their symbols.

Table 5

The different state of the system with faults and their symbols.

Faults	Symbols
Healthy system	Class 1
Two PV modules short circuit	Class 2
Five PV modules short circuit	Class 3
Two inversed By-pass diodes	Class 4
Ground fault	Class 5
Open circuit PV branch	Class 6

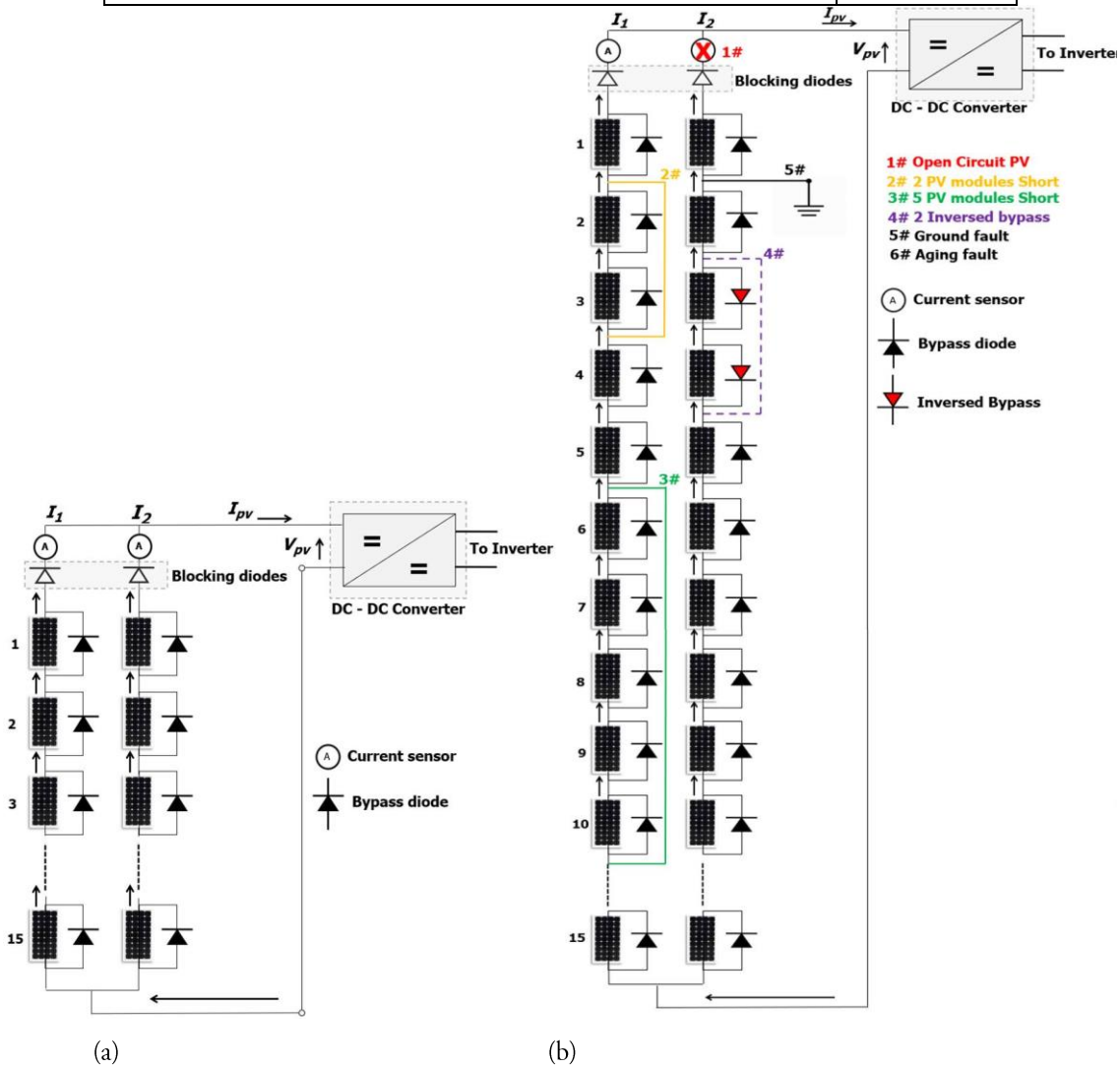

Fig. 4. Overall scheme of the PV array (a) healthy PV array (b) faulty PV array.

The description of various classes treated in this study, their combinations and their corresponding codes are in accordance with Tables 5 and 6 respectively. The demonstration of classification analysis and diagnosis are based on the percentage linear scatter plot of both current and voltage of maximum power point and are clearly demonstrated by the flowcharts in Fig. 5 where the flowchart (a) is designed to detect the fault and the second flowchart (b) is designed to identify and isolate five faulty cases citing: 1) Two PV modules short circuit, 2) Five PV modules short circuit, 3) Two inversed By-pass diodes, 4) ground fault and 5) Open circuit PV branch. Where each case in the two flowcharts contain its own signature presented under percentage deviation between experimental and predicted data in addition to the threshold that are considered as a confidence interval in the aim to avoid the overlap between signatures of different faults. Table 8 illustrates the fault classes codes treated in this article and their relative deviation symbols.

Table 6

Classes' description and codes.

Classes description	Codes
Maximum power point current of healthy conditions	C1I
Maximum power point current of open circuit PV branch	C2I
Maximum power point voltage of heathy conditions	C1V
Maximum power point voltage of two PV module short circuit	C2V
Maximum power point voltage of five PV modules short circuit	C3V
Maximum power point voltage of two inversed By-pass diode	C4V
Maximum power point voltage of ground fault	C5V

Table 7

Different combination of classes obtained.

Impp Class	Vmpp Class	Global Description	Global Classification
C1I	C1V	Healthy system	Class1
C1I	C2V	Two PV modules short circuit in Branch	Class 2
C1I	C3V	Five PV modules short circuit in Branch	Class 3
C1I	C4V	Two inversed By-pass diodes in PV Branch	Class 4
C1I	C5V	Ground fault in PV branch	Class 5
C2I	C1V	Open circuit fault in PV branch	Class 6

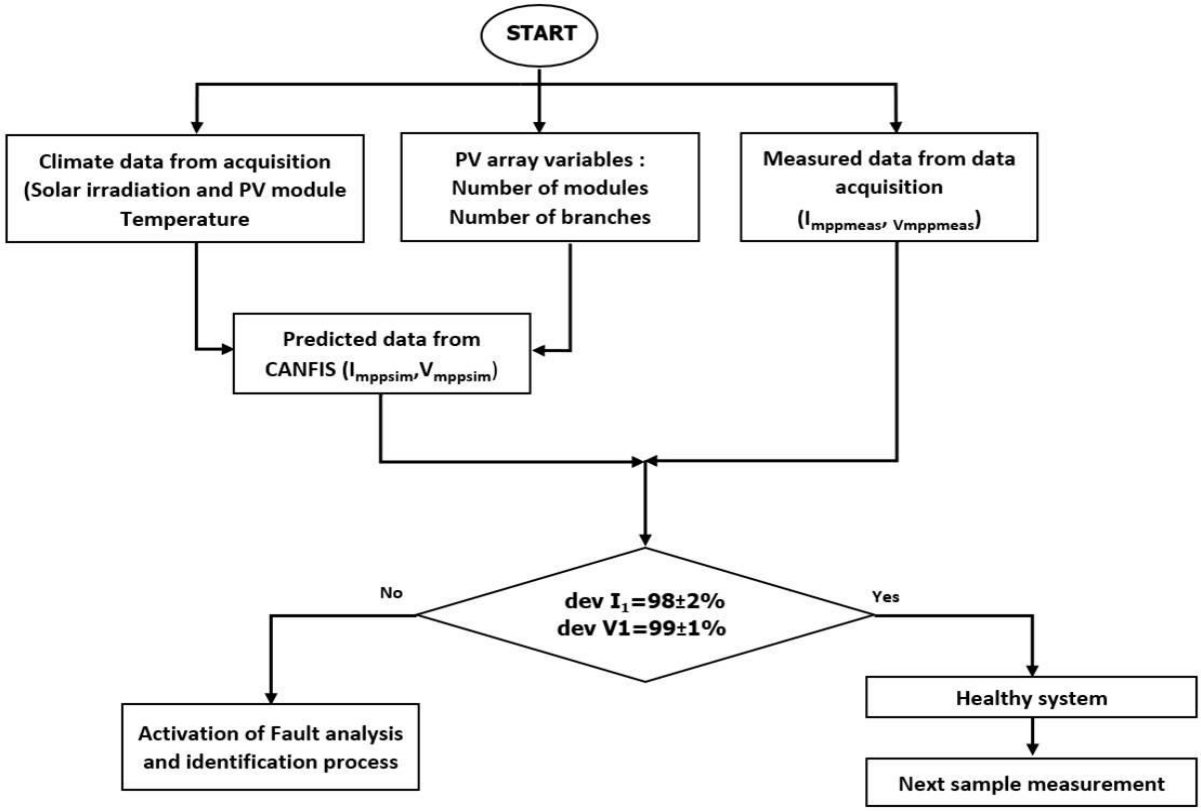

(a)

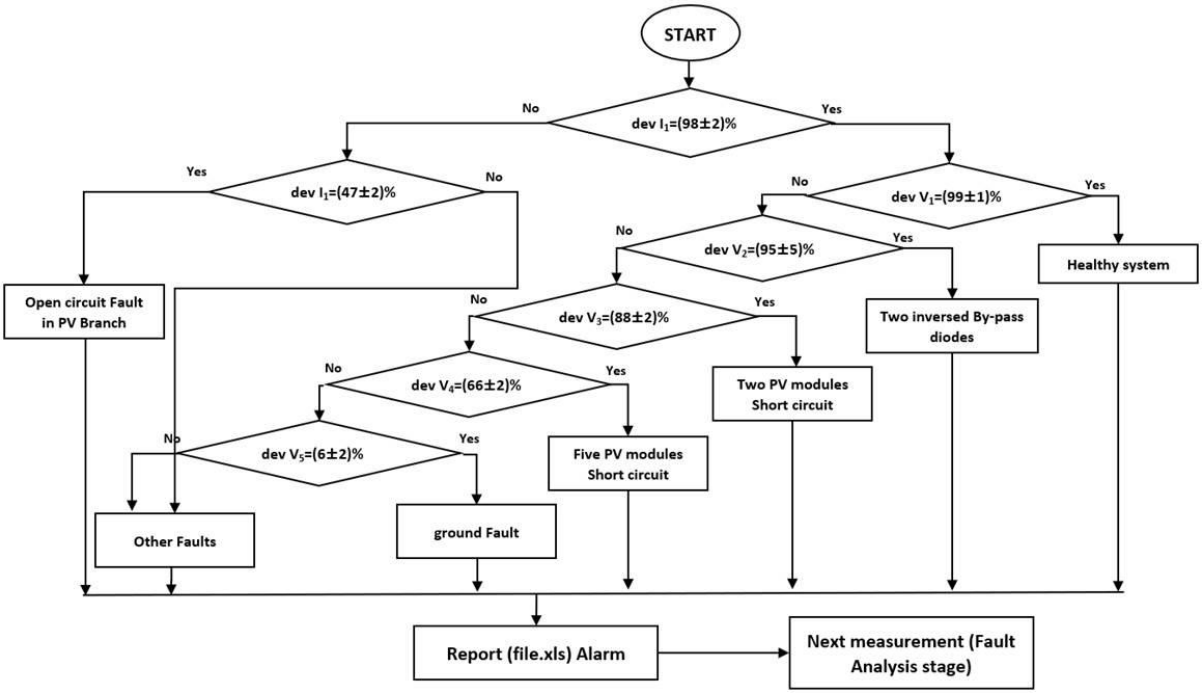

(b)

Fig. 5. Flowchart of the diagnosis algorithm (a) fault detection (b) global diagnosis, of PV system.

Table 8

Deviation symbols with their relative classes codes.

Deviation symbols	**Dev I1**	**Dev I2**	**Dev V1**	**Dev V2**	**Dev V3**	**Dev V4**	**Dev V5**
Classes codes	C1I	C2I	C1V	C2V	C3V	C4V	C5V

5. Results presentation and discussion

5.1. Model development and training

In order to guarantee the fault diagnosis of PV system, the training phase of developed model (CANFIS) has been done with two input data and two output data where each attributes contains 3000 samples for the six classes treated in this study. The important parameters required by CANFIS algorithm are illustrated in the Table 9 below:

Table 9

Parameters of the CANFIS algorithm

CANFIS parameters	
Input data	**2 (Solar irradiation, PV module Temperature)**
Output data	**2 (Current and voltage of maximum power point)**
Fuzzy model	**TKS (Takagie-Suegeno)**
Membership functions (MFs)	**Gaussian Membership functions**
MFs	**2 MFs per input variable**
Number of rules	**2**
Error goal	**0.001**
epochs	**1000**
Momentum	**0.65**
Output membership function	**linear**
Learning algorithm for adjusting parameters	**Hybrid**

5.2. Healthy case

5.2.1. Voltage

Part (a) of Figs. 6, 7 and 8 corresponds to line graphs between healthy measured voltage and predicted healthy voltage from CANFIS algorithm for training, checking and testing phases respectively, where the results shown a perfect concordance between both models. Voltage's gap in part (b) in the same figures cited above in this section reveal a good results between (-15, +15 V) comparing to the global voltage of the healthy PV array. While the scatter plot in linear percentage deviation between real measured data and predicted CANFIS data for healthy voltage is around 99% in part (c) of all figures of section (5-1-1) which is an excellent result. From the results proved in this

section, it can be evident to say that voltage's CANFIS algorithm has shown beyond doubt a significant level in term of accuracy and efficiency and it is able to be used for other faulty voltage in PV array that we will demonstrate in the next sections.

a. Training

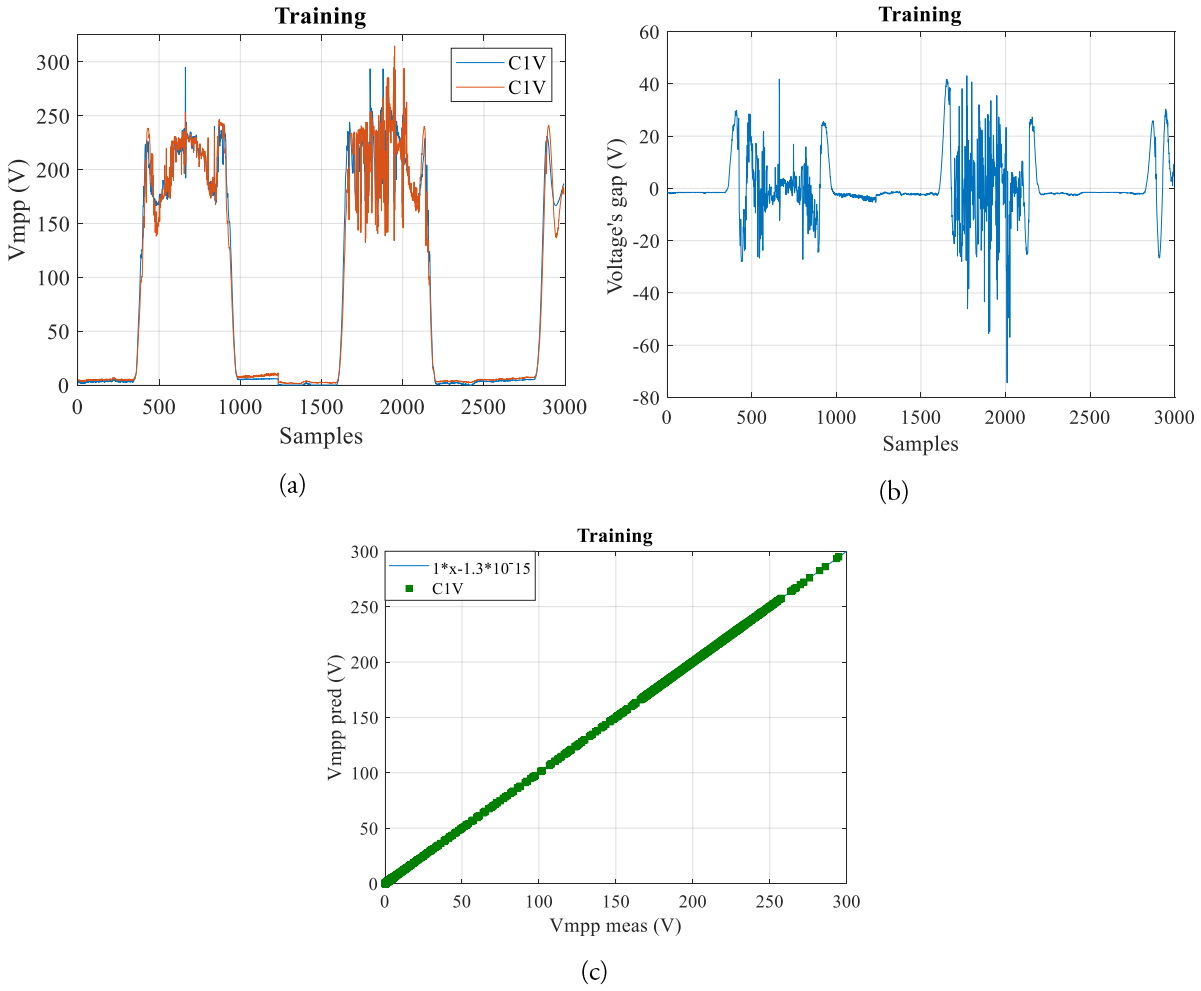

Fig. 6. Real versus predicted healthy voltage of training phase.

b. Checking

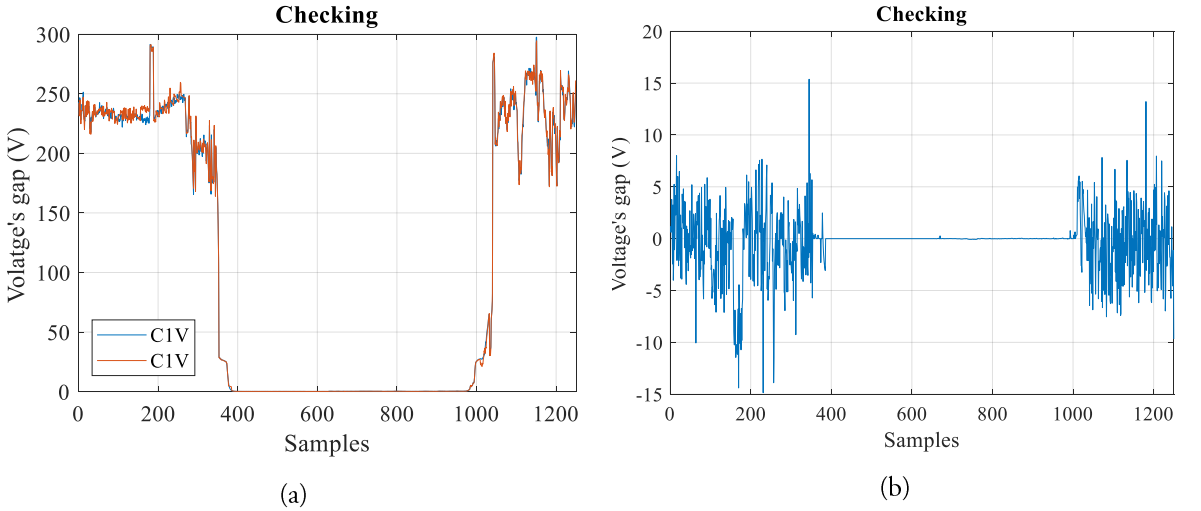

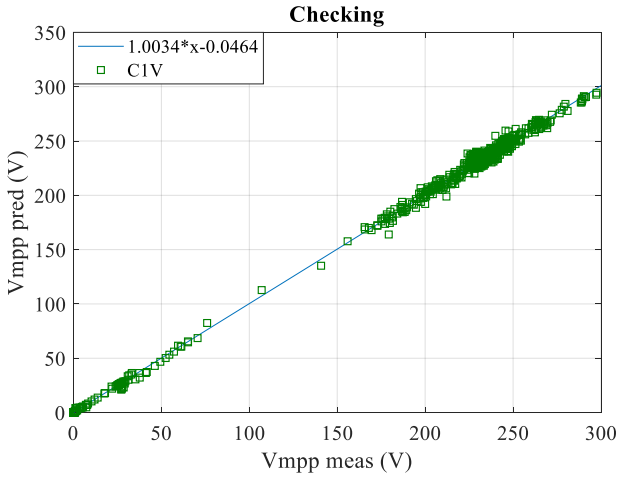

(c)

Fig. 7. Real versus predicted healthy voltage of checking phase.

c. Testing

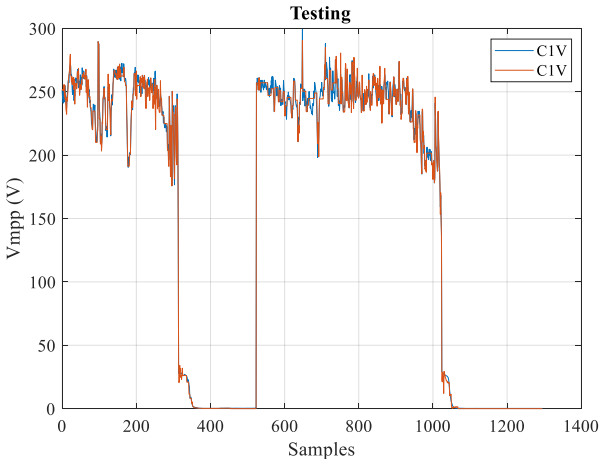

(a)

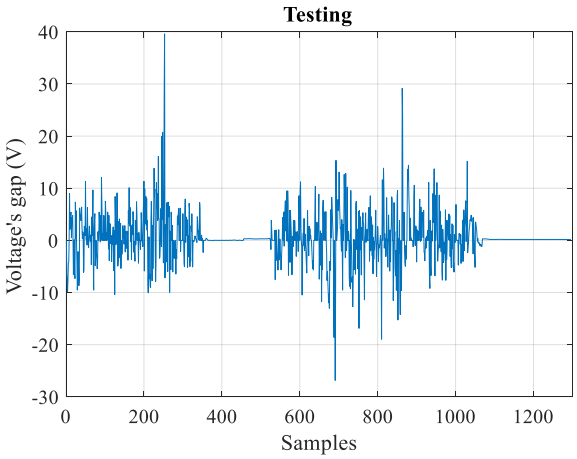

(b)

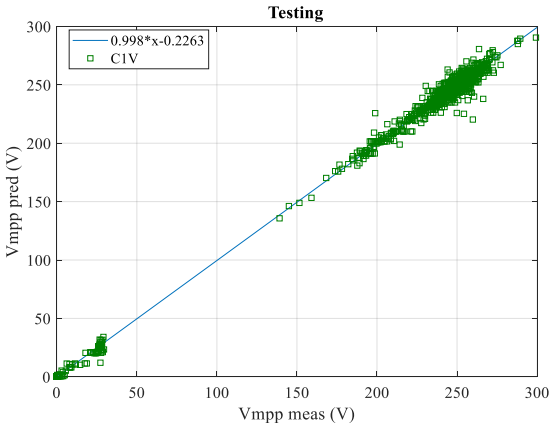

(c)

Fig. 8. Real versus predicted healthy voltage of testing phase.

5.2.2. Current

In this section, the line graphs between healthy measured current and predicted healthy current from CANFIS algorithm for training, checking and testing phases respectively illustrated in part (a) of Figs. 9, 10 and 11 reveal an impeccable correspondence between both models. In the other hand, the current's gap in part (b) in the same figures of the actual section is apparent with low margin of error which is in average between (-0.5, 0.5 A) comparing to the overall current of the healthy PV array. When to the part (c) of the same figures in this section, the scatter plot in linear percentage deviation between real measured data and predicted CANFIS data for healthy current is around 98% which represents a remarkable result. According to the results shown in the figures of the present section, current's CANFIS algorithm has confirmed an excellent quality from precision and efficiency point of view that can be taken in consideration for other faulty current.

a. Training

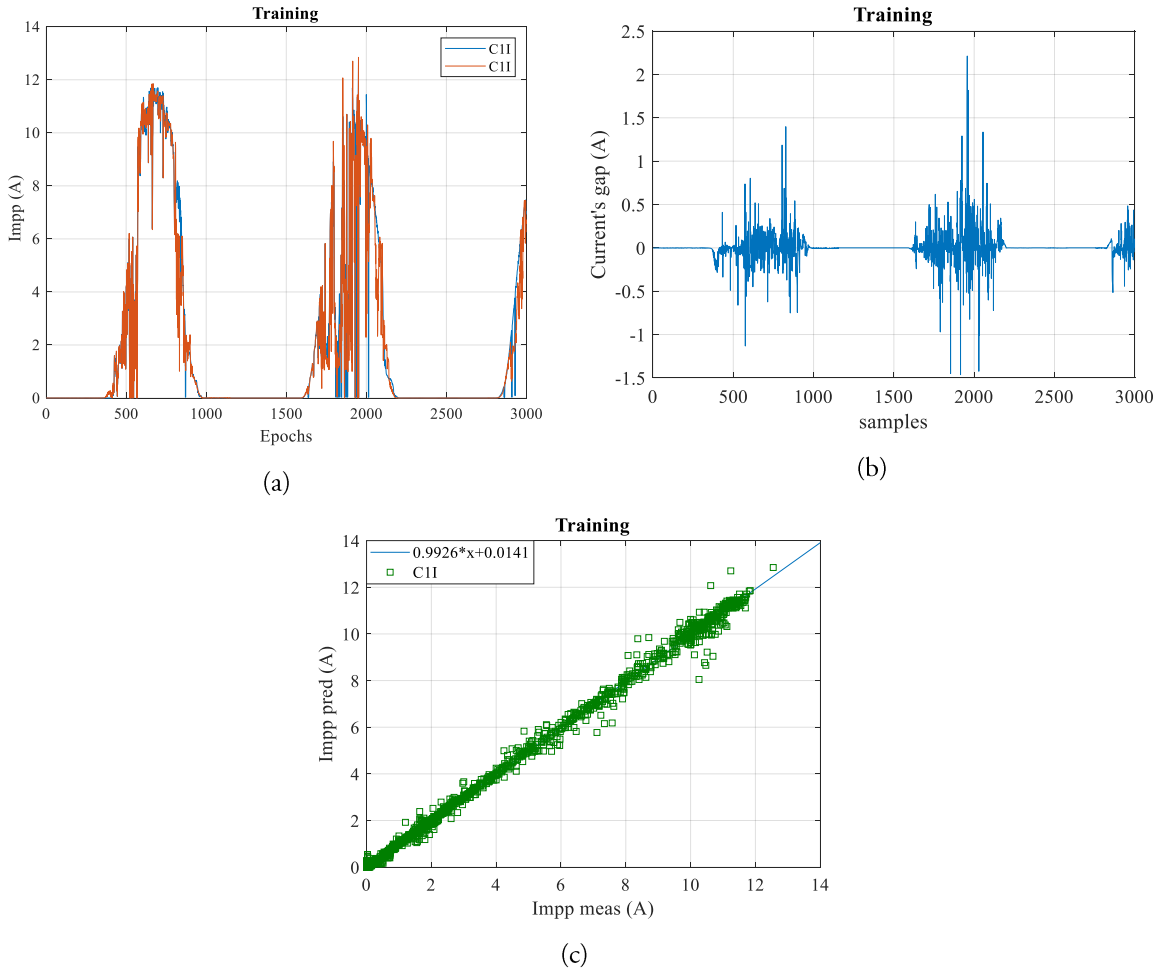

Fig. 9. Real versus predicted healthy current of training phase.

b. Checking

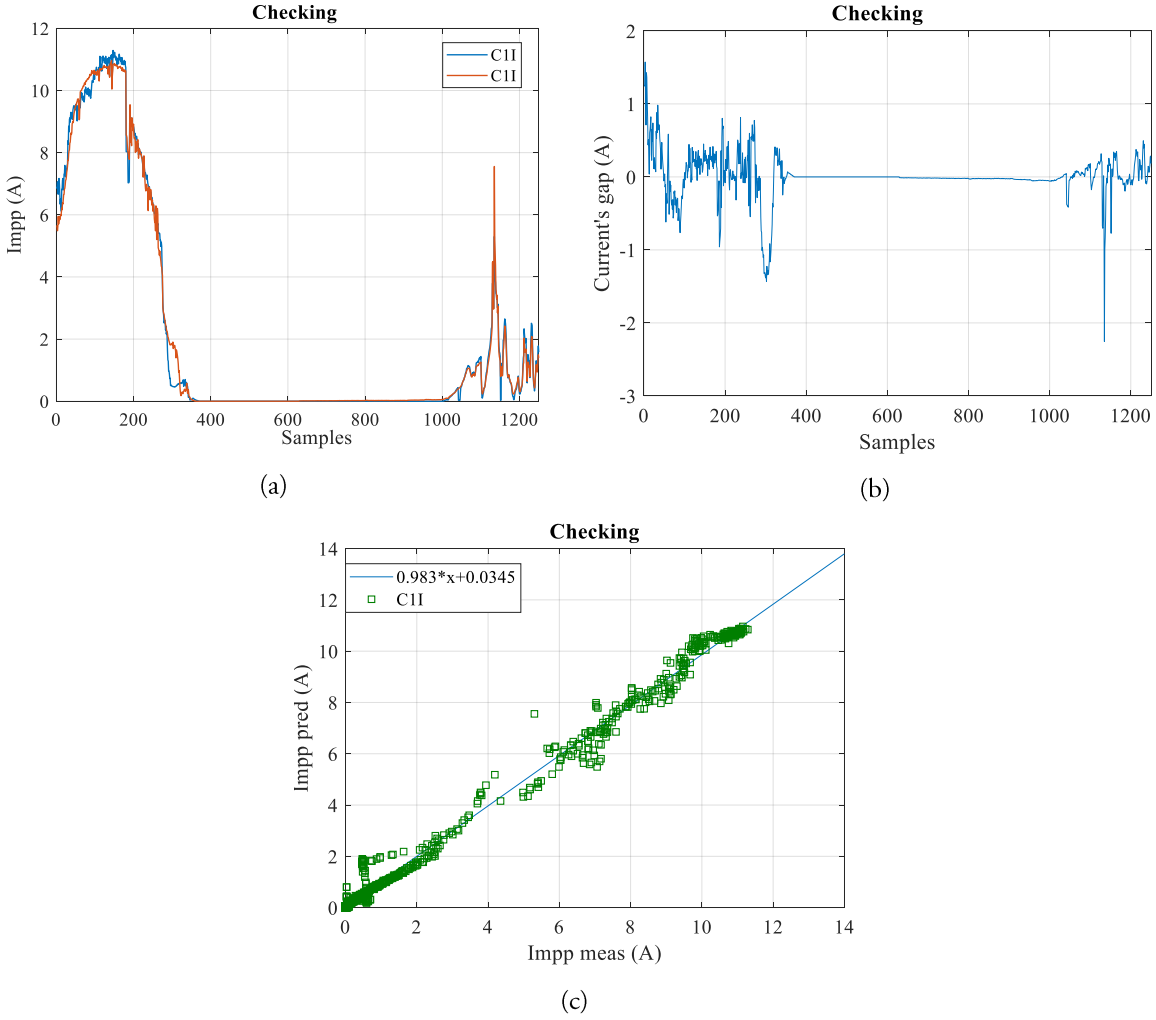

Fig. 10. Real versus predicted healthy current of checking phase.

c. Testing

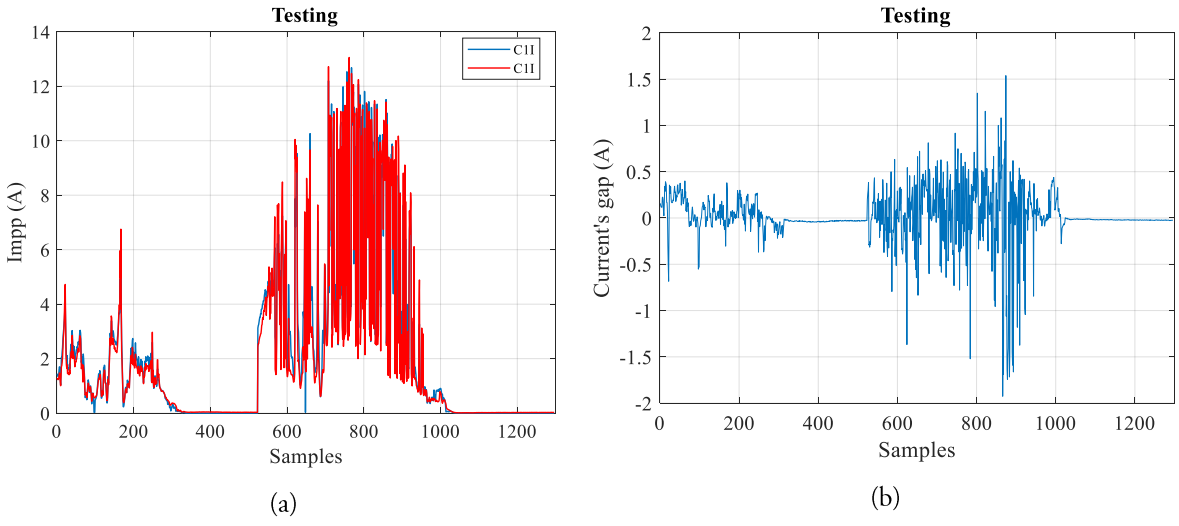

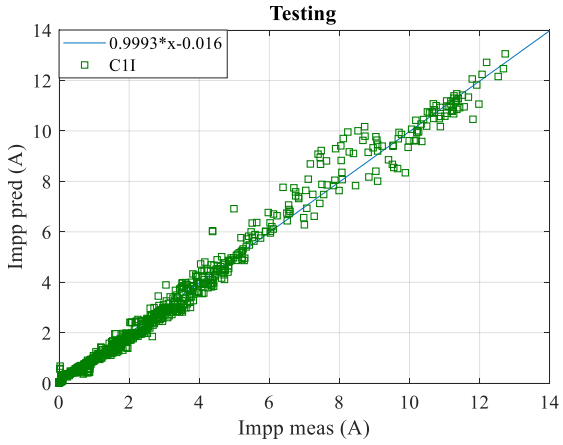

(c)

Fig. 11. Real versus predicted healthy current of testing phase.

5.2.3. Performance analysis of the CANFIS algorithm

The principal aim of the Fig. 12 is to prove the performance evaluation of the CANFIS algorithm results by the employment of residual criteria cited previously for the healthy voltage and current at maximum power point of PV array comparing to the real measured data. It's clear to note that the model has furnished a high quality in term of precision whether for the voltage or for the current. In this part, Fig. 12 (a) represents the MSE displaying 0, 7.53, 19.89 and 0.026, 2.88, 15.18 in training, checking and testing phases for both Vmpp and Impp respectively. While Fig. 12 (b) illustrates the RMSE where the results are: 0, 0.16, 4.46 and 0.16, 5.36, 3.89 for Vmpp and Impp in training, checking and testing phases respectively. MAPE is demonstrated in Fig. 12 (c), the results here are: 0, 2.80, 2.79 for Vmpp and 3.70, 4.65, 4.59 for Impp in the three phases respectively (training, checking and testing). MAD in Fig. 12 (d) displays 0.75, 1.48, 2.54 for Vmpp and 0.061, 1.28, 4.98 for Impp in training, checking and testing phases respectively. In Fig. 12 (e), the results are as follow: 0.999, 0.999, 0.998 for Vmpp and 0.997, 0.994, 0.99 for Impp in the three phases (training, checking and testing). The Table 10 below illustrates the average ± Standard Deviation (SD) of R^2 for both Vmpp and Impp in training, checking and testing phases.

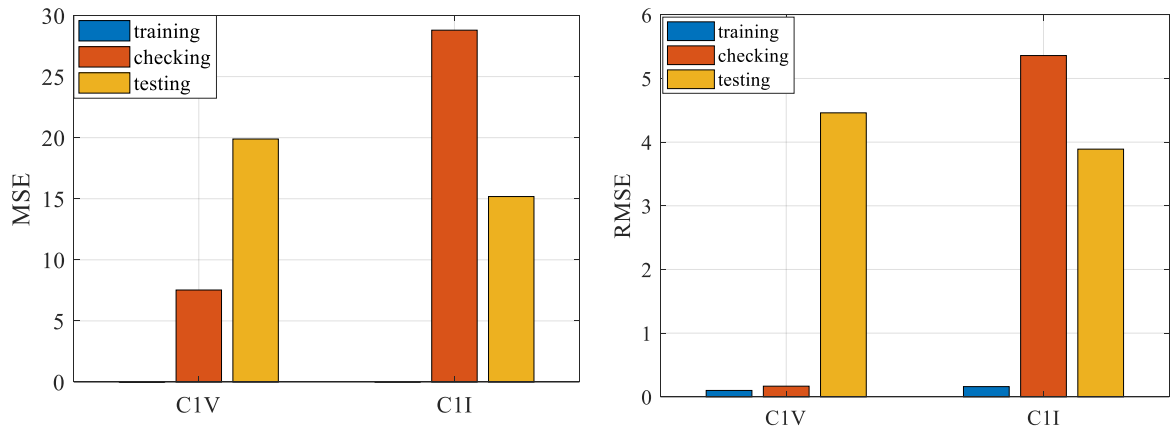

(a) (b)

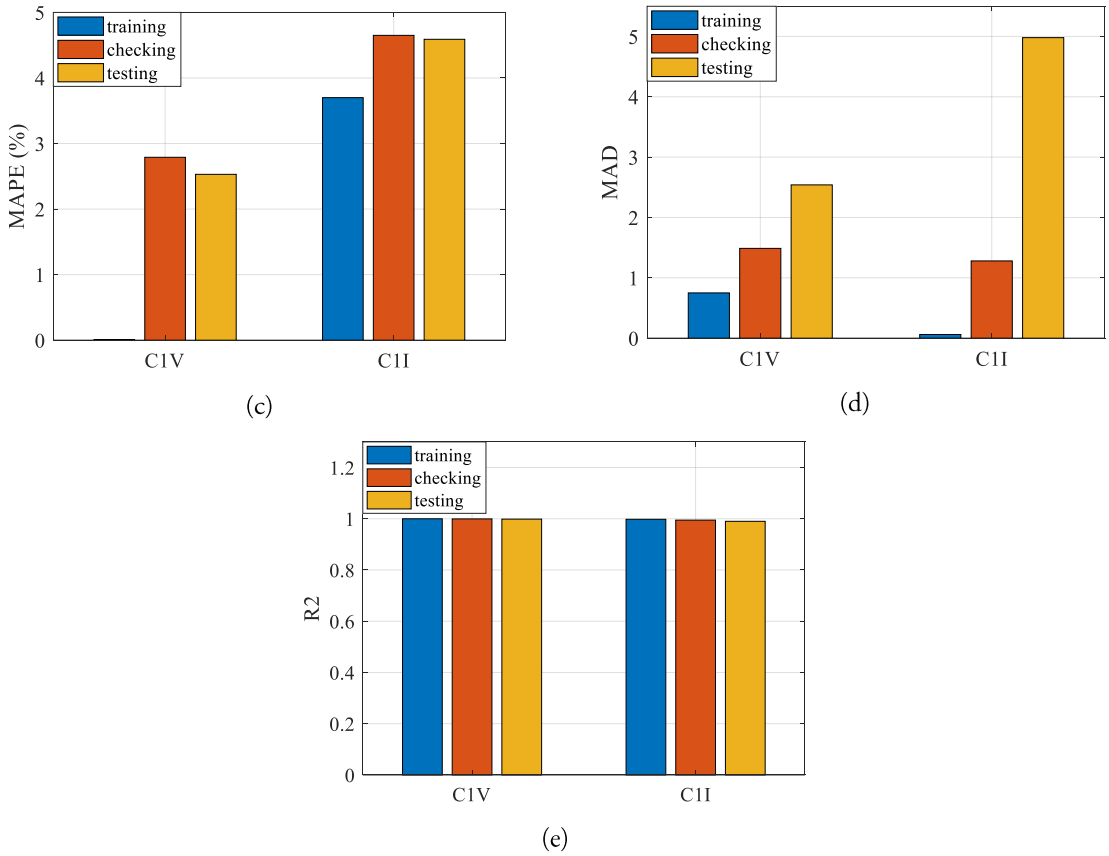

Fig. 12. Global residual criteria of Vmpp and Impp for healthy case.

Table 10

R2 Standard deviation of the CANFIS algorithm.

	Training	Checking	Testing
Average ± SD (Vmpp)	0.999 ± 9.57 x 10^{-5}	1 ± 2.17 x 10^{-3}	0.999 ± 8.57 x 10^{-4}
Average ± SD (Impp)	0.997± 4.75 x 10^{-3}	0.994± 8.58 x 10^{-3}	0.99± 8.38 x 10^{-4}

5.3. Two PV modules short circuited

5.3.1. Voltage

It is clear to observe the few difference between the healthy measured voltage and the predicted of two PV modules short circuit fault from CANFIS algorithm in Part (a) of Figs. 13, 14 and 15 corresponding to line graphs for training, checking and testing phases which is of the order of the tenth. Voltage's gap in part (b) in the same figures cited above in the present section demonstrates the difference between healthy measured voltage and the predicted voltage of the present fault which is in average between (20 and 35 V) in the three phases (training, checking and testing). While the scatter plot in linear percentage deviation between the real healthy measured data and the predicted from CANFIS algorithm of two PV modules short circuit fault is around 88% in part (c) of all figures in the current section for training, checking and testing phases respectively.

a. Training

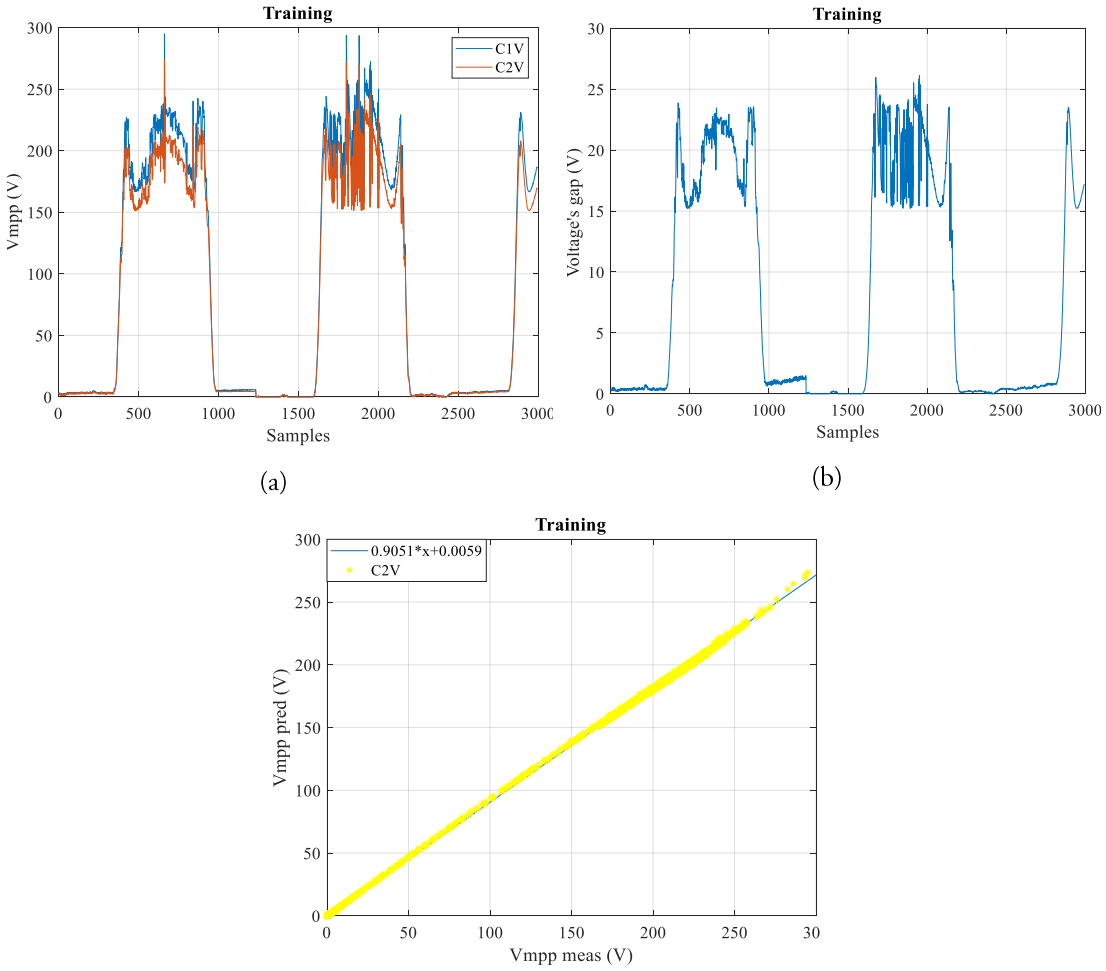

Fig. 13. Real healthy versus predicted two PV modules short circuit voltage of training phase.

b. Checking

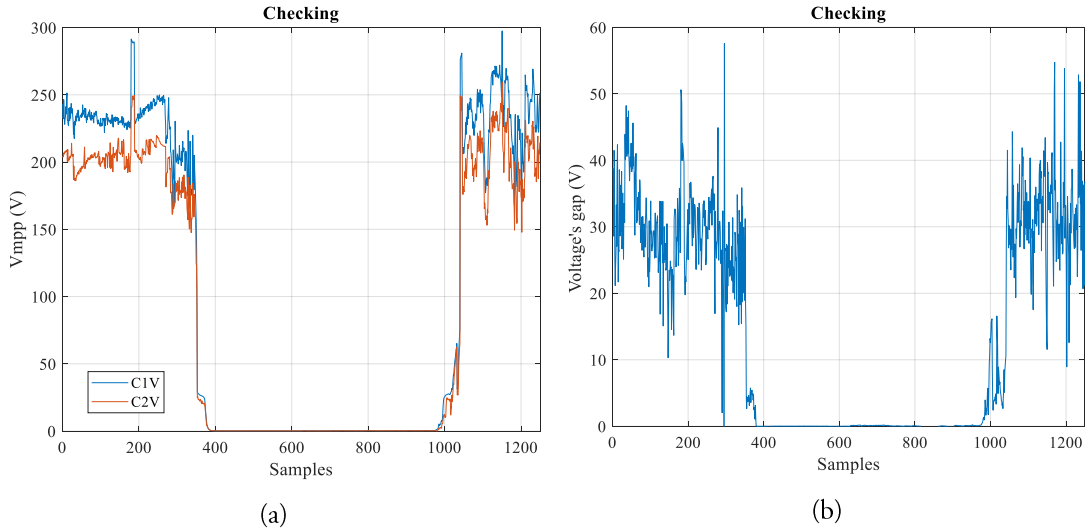

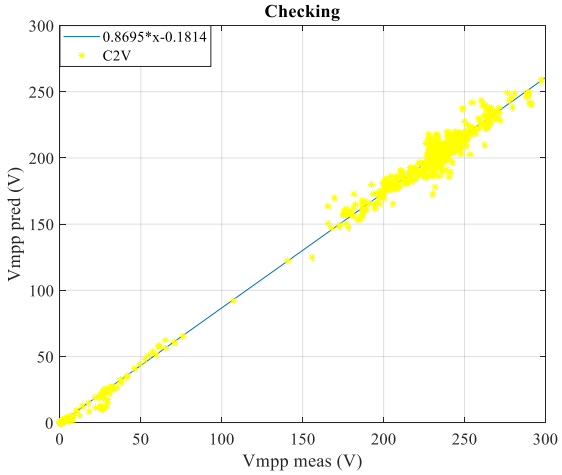

(c)

Fig. 14. Real healthy versus predicted two PV modules short circuit voltage of checking phase.

c. Testing

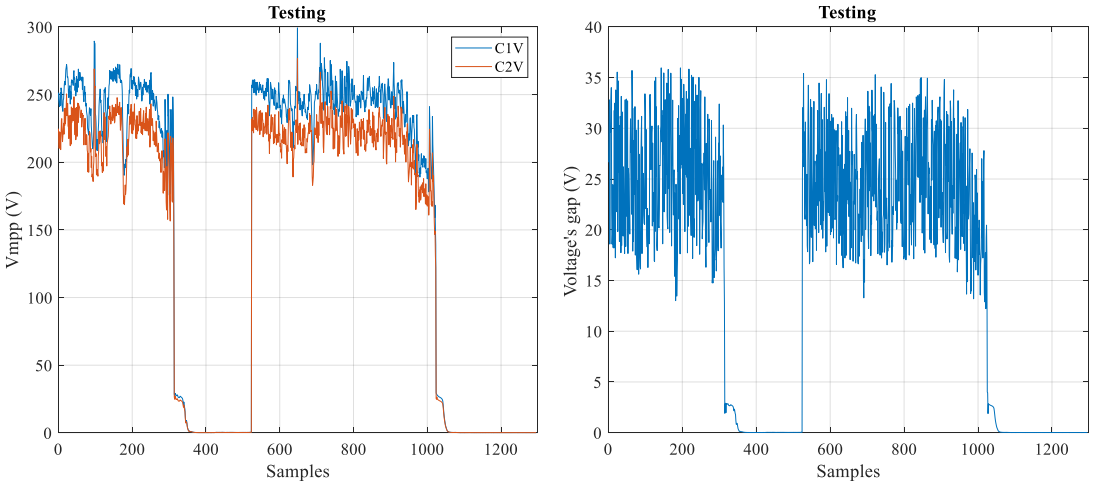

(a)

(b)

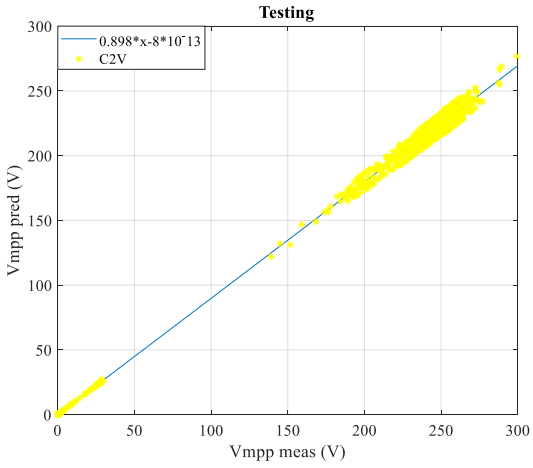

(c)

Fig. 15. Real healthy versus predicted two PV modules short circuit voltage of testing phase.

5.3.2. Current

In this case, the current values at maximum power point is the same as in section 5-1-2 with negligible change that cannot be observed.

5.4. Five PV modules short circuited

5.4.1. Voltage

In Part (a) of Figs. 16, 17 and 18 the predicted voltage of five PV modules short circuit fault from CANFIS algorithm corresponding to line graphs for training, checking and testing phases diminishes by the one third comparing to the healthy real measured voltage. When the Voltage's gap in part (b) in the same figures cited in the present section illustrates the difference between healthy measured voltage and the predicted voltage of the actual fault which is in average between (60 and 80 V) in the three phases (training, checking and testing). The scatter plot in linear percentage deviation between the real healthy measured data and the predicted from CANFIS algorithm of five PV modules short circuit fault is around 66% in part (c) in all figures of the section (5-3-1) for training, checking and testing phases.

a. Training

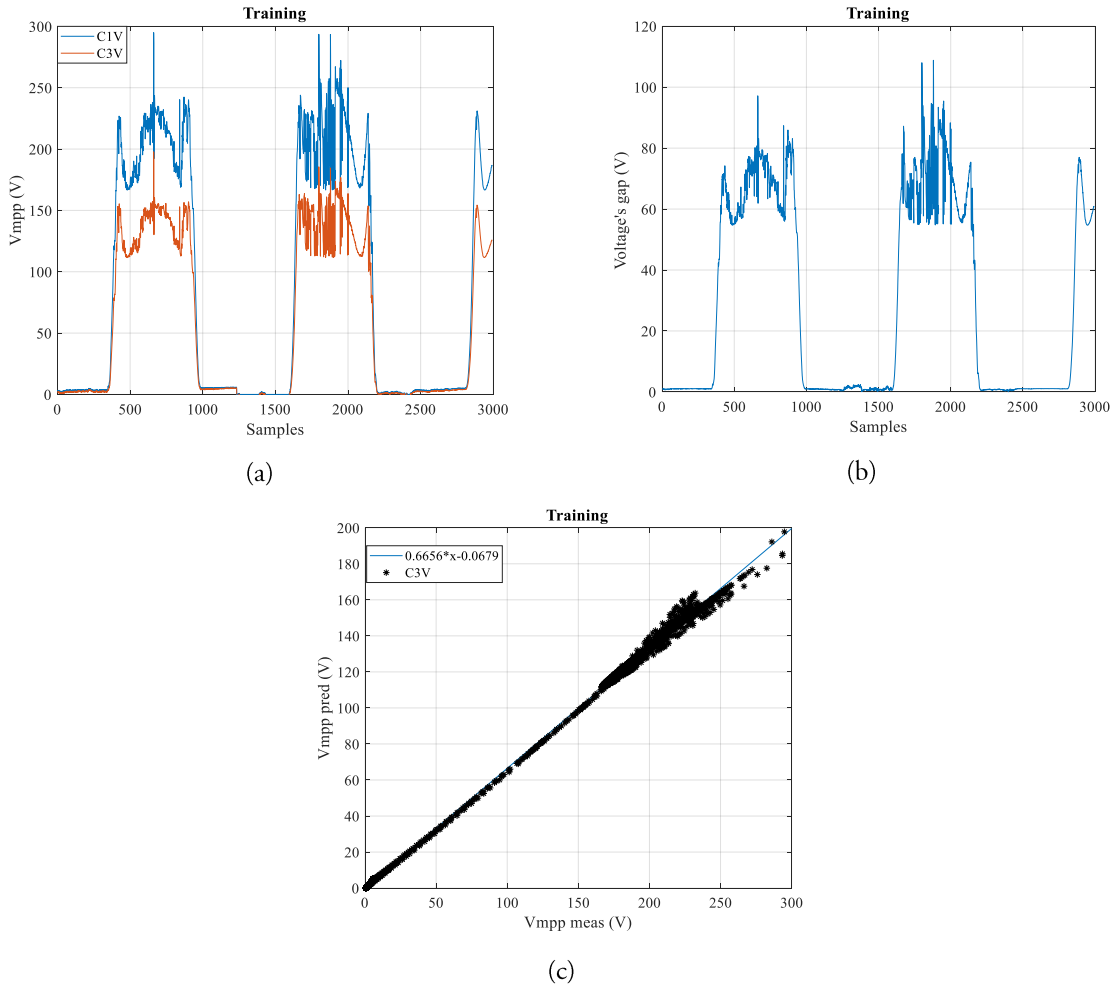

Fig. 16. Real healthy versus predicted five PV modules short circuit voltage of training phase.

b. Checking

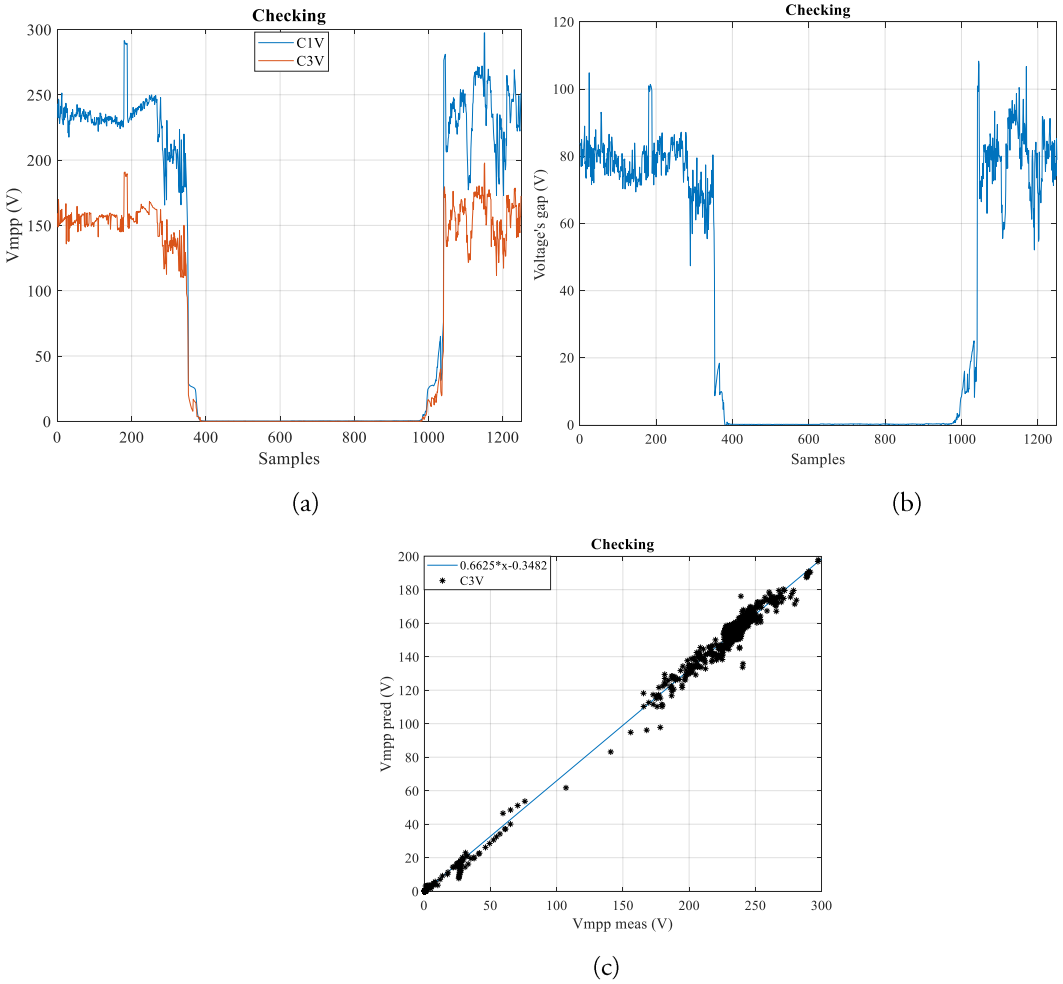

Fig. 17. Real healthy versus predicted five PV modules short circuit voltage of checking phase.

c. Testing

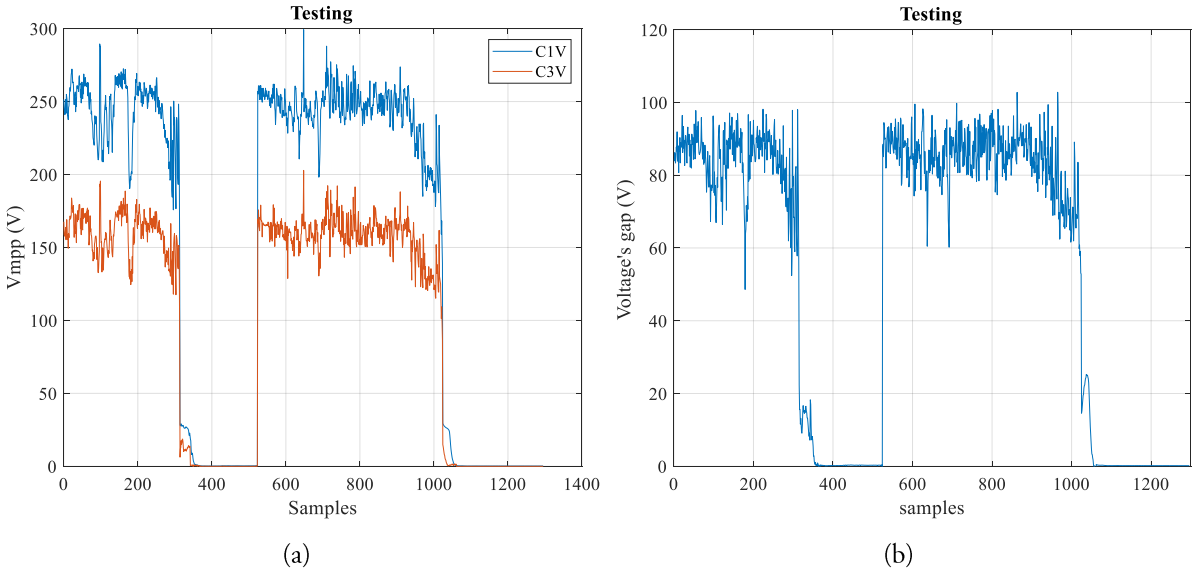

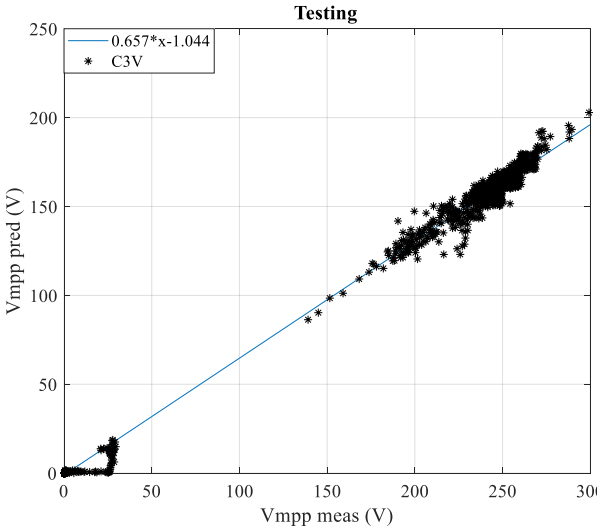

(c)

Fig. 18. Real healthy versus predicted five PV modules short circuit voltage of testing phase.

5.4.2. Current

In this case, the current values of Maximum power point is the same as in section 4-1-2 with negligible change that cannot be observed.

5.5. Two inversed By-pass Diodes

5.5.1. Voltage

An important number of samples of the predicted two inversed by-pass diodes fault from CANFIS algorithm are in overlap with healthy measured data in Part (a) of Figs. 19, 20 and 21 corresponding to line graphs for training, checking and testing phases which is difficult to separate the difference between both classes. Voltage's gap in part (b) in the same figures cited above in the present section demonstrates the difference between healthy measured voltage and the predicted voltage of the present fault which is in average between (6 and 18 V) in the three phases (training, checking and testing). While to the scatter plot in linear percentage deviation between the real healthy measured data and the predicted of two inversed by-pass diodes fault from CANFIS algorithm is around 95 % in part (c) of all figures in the present section for training, checking and testing phases.

a. Training

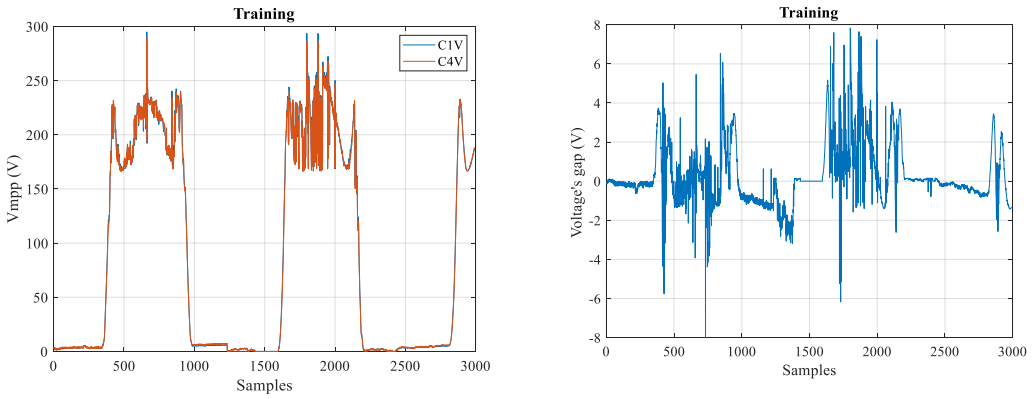

(a) (b)

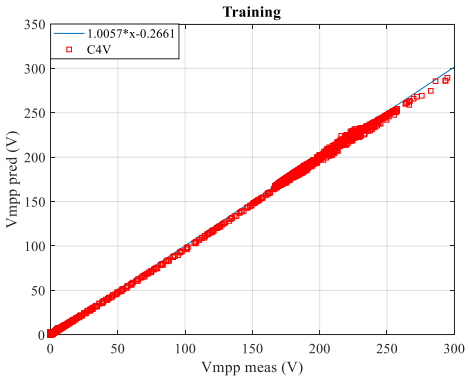

(c)

Fig. 19. Real healthy versus predicted two inversed by-pass diodes voltage of training phase.

b. Checking

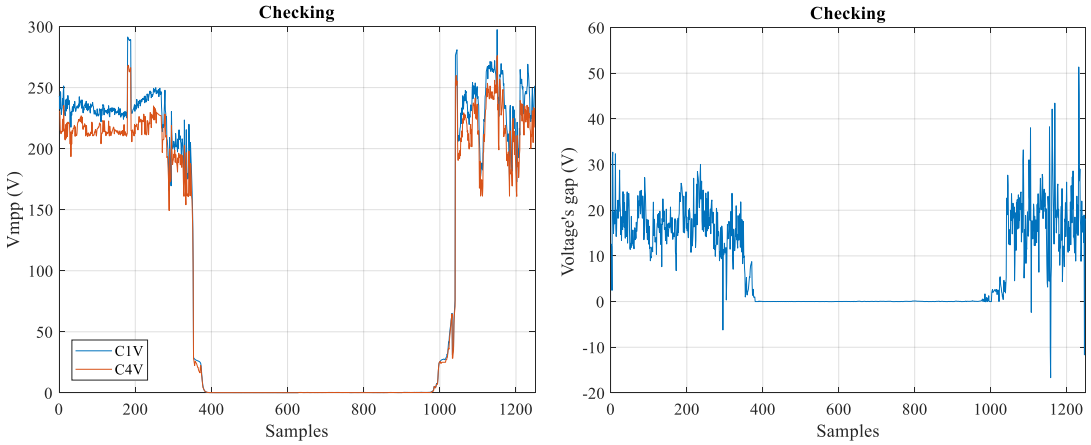

d. (a) (b)

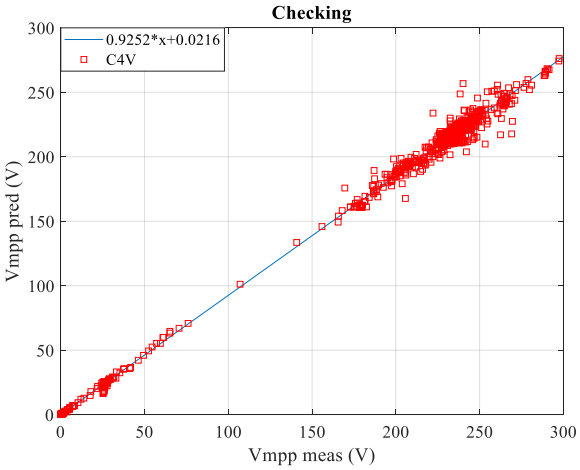

(c)

Fig. 20. Real healthy versus predicted two inversed by-pass diodes voltage of checking phase.

e. Testing

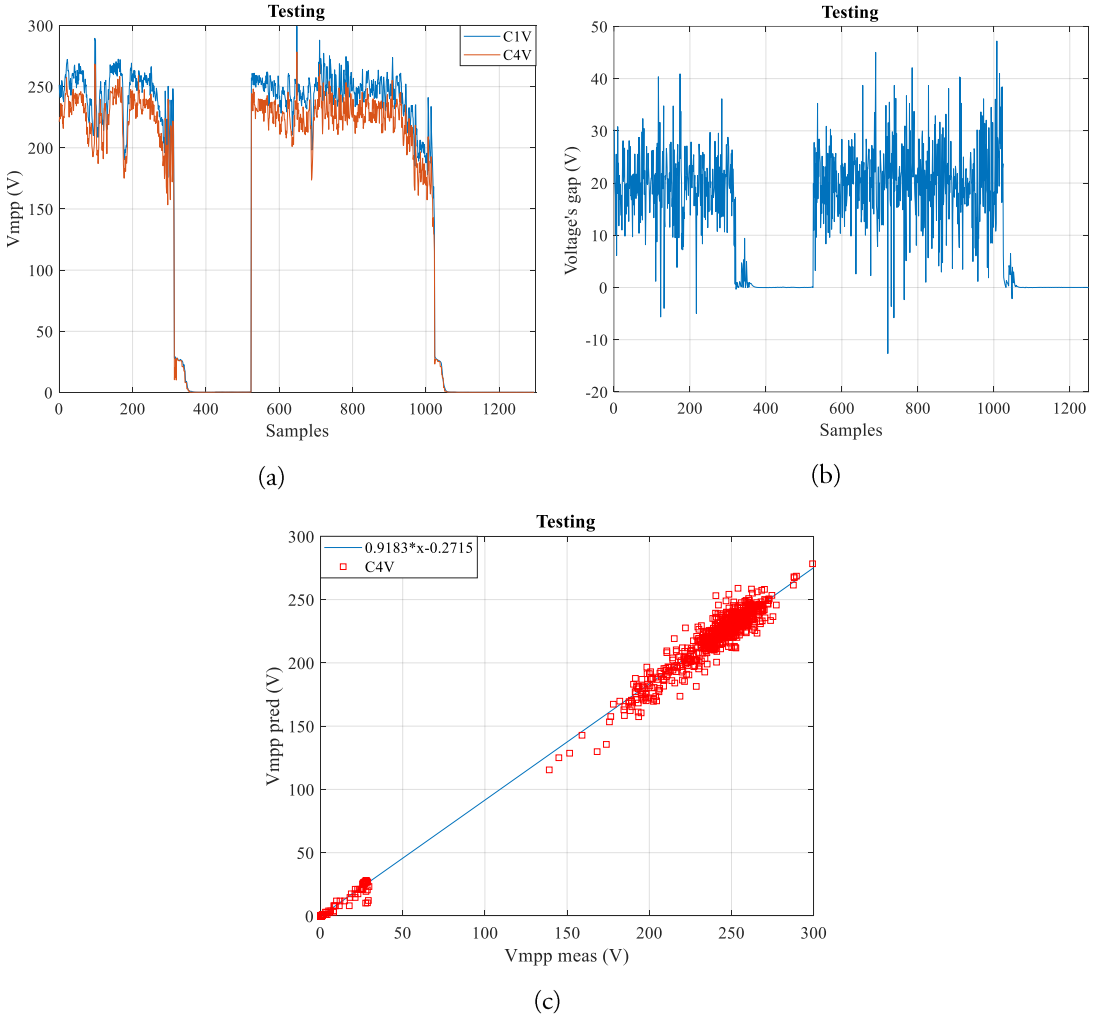

Fig. 21. Real healthy versus predicted two inversed by-pass diodes voltage of testing phase.

5.5.2. Current

In this case, the current values at Maximum power point is the same as in section 5-1-2 with negligible change that cannot be spotted.

5.6. Ground fault

5.6.1. Voltage

It is noteworthy to do the difference in Part (a) of Figs. 22, 23 and 24 between healthy real measured data and the predicted voltage of ground fault from CANFIS algorithm corresponding to line graphs for training, checking and testing phases where the lowering is of the order of the one-fifth . When the Voltage's gap in part (b) in the same figures cited in the present section illustrates the difference between healthy measured voltage and the predicted voltage of the actual fault which is in average between (200 and 250 V) in the three phases (training, checking and testing). The scatter plot in linear percentage deviation between the real healthy measured data and the predicted of ground fault CANFIS algorithm is around 7% in part (c) of all figures in section (5-5-1) for training, checking and testing phases.

a. Training

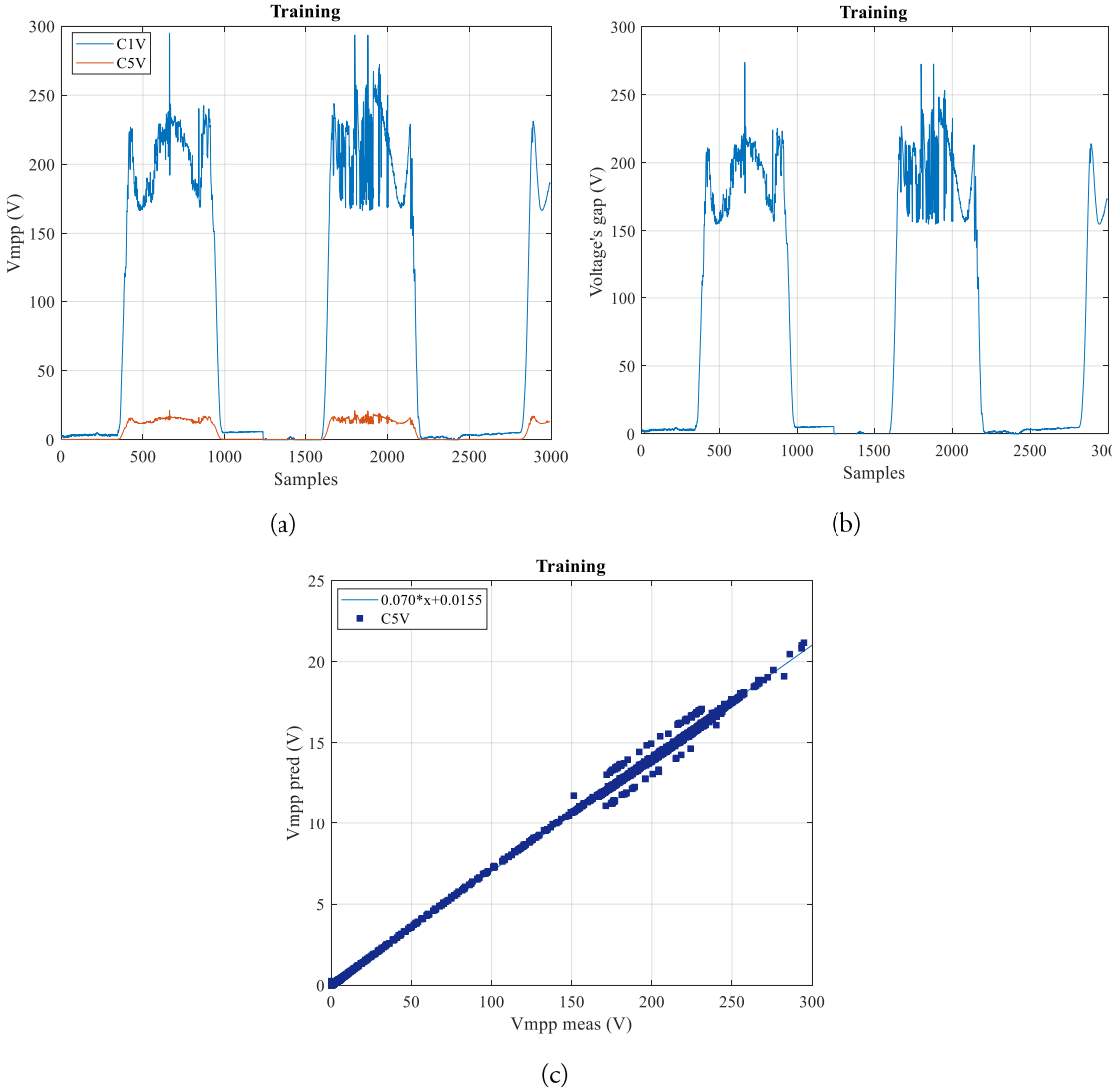

Fig. 22. Real healthy versus predicted ground fault voltage of training phase.

b. Checking

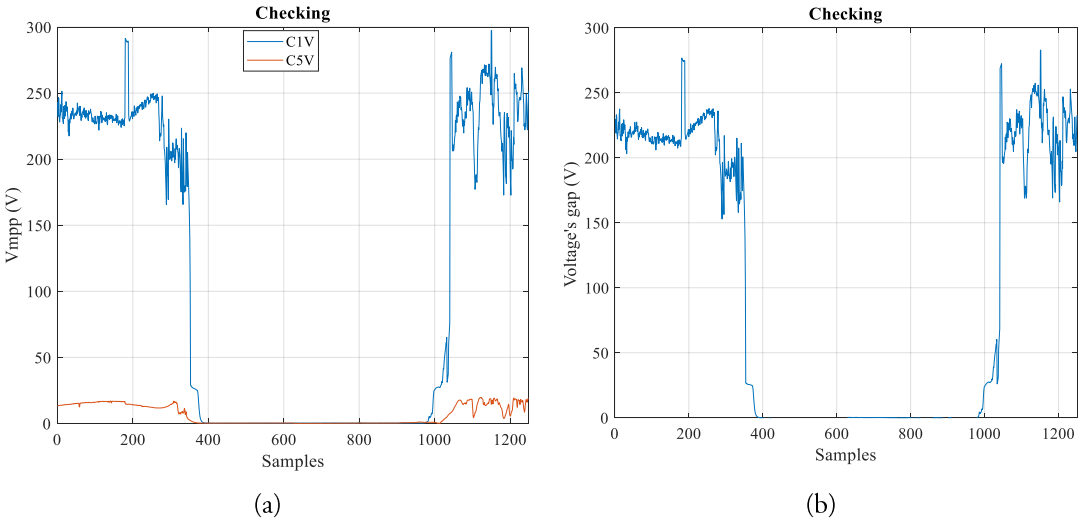

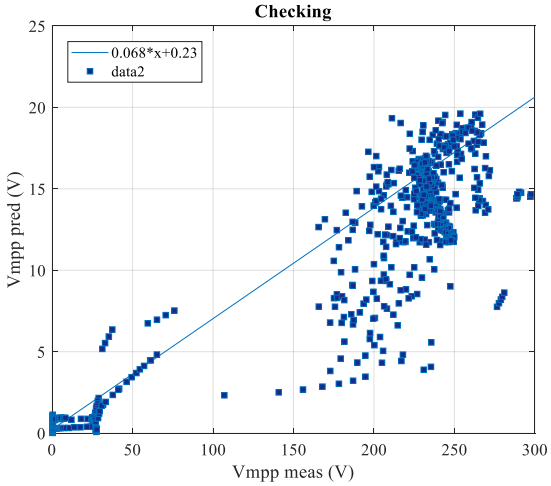

(c)

Fig. 23. Real healthy versus predicted ground fault voltage of checking phase.

c. Testing

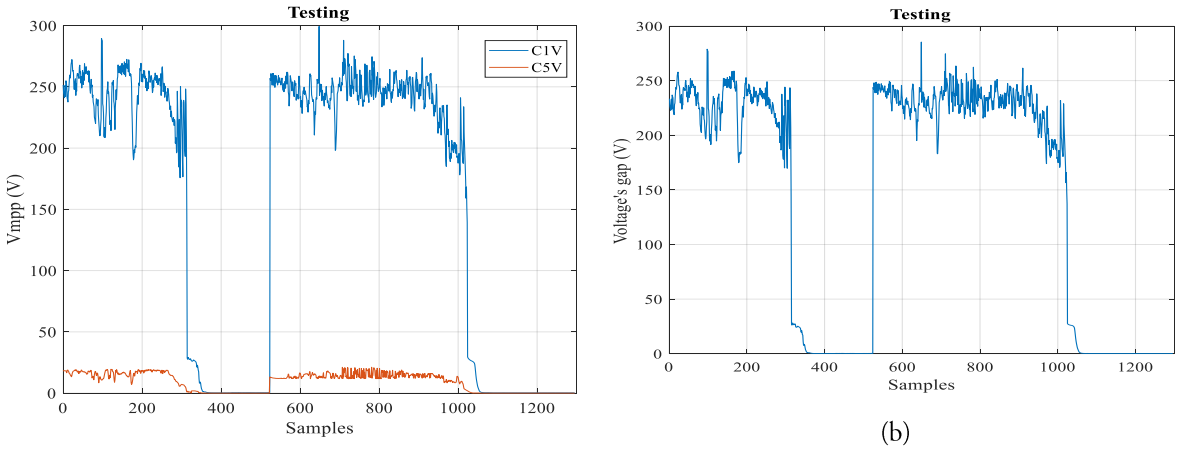

(a) (b)

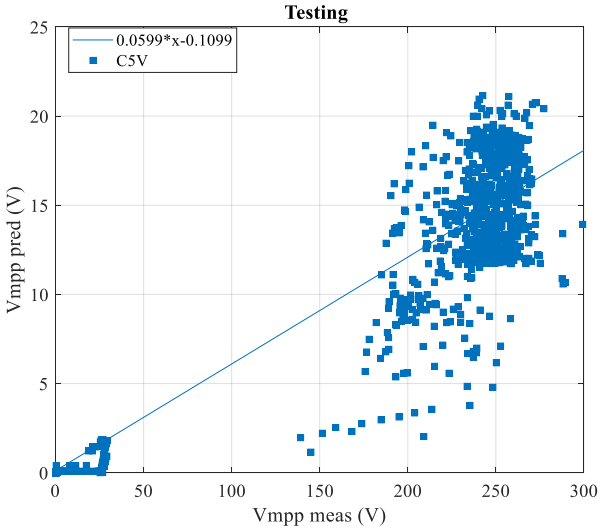

(c)

Fig. 24. Real healthy versus predicted ground fault voltage of checking phase.

5.6.2. Current

In this case, the current values at maximum power point is the same as in section 5-1-2 with negligible change that cannot be remarked.

5.7. Disconnected string

5.7.1. Voltage

In this case, the voltage values at maximum power point is the same as in section 5-1-1 with negligible change that cannot be distinguished.

5.7.2. Current

The line graphs in part (a) of Figs. 25, 26 and 27 between healthy measured current and predicted from CANFIS algorithm of open circuit branch fault in PV array for training, checking and testing phases demonstrated the difference between both classes where the current of this fault has decreased by half comparing to the healthy . From current's gap point of view in part (b) of the same figures in this present section, which is the difference between healthy and open circuit fault is around half comparing to healthy current. When to the part (c) of all figures in section (5-5-2), the scatter plot in linear percentage deviation between healthy real measured data and predicted CANFIS data for open circuit fault (C2V) is around 46%.

a. Training

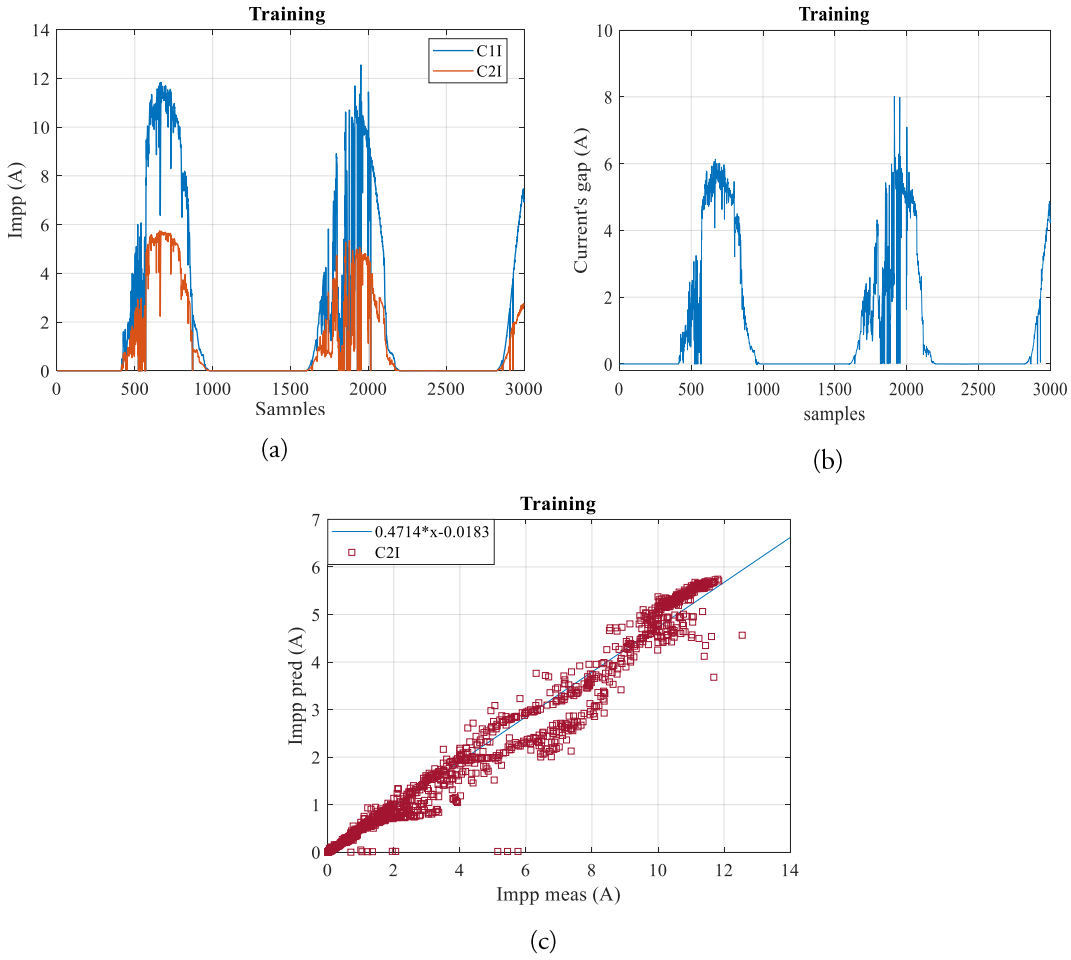

Fig. 25. Real healthy versus predicted open circuit branch in PV array of training phase.

b. Checking

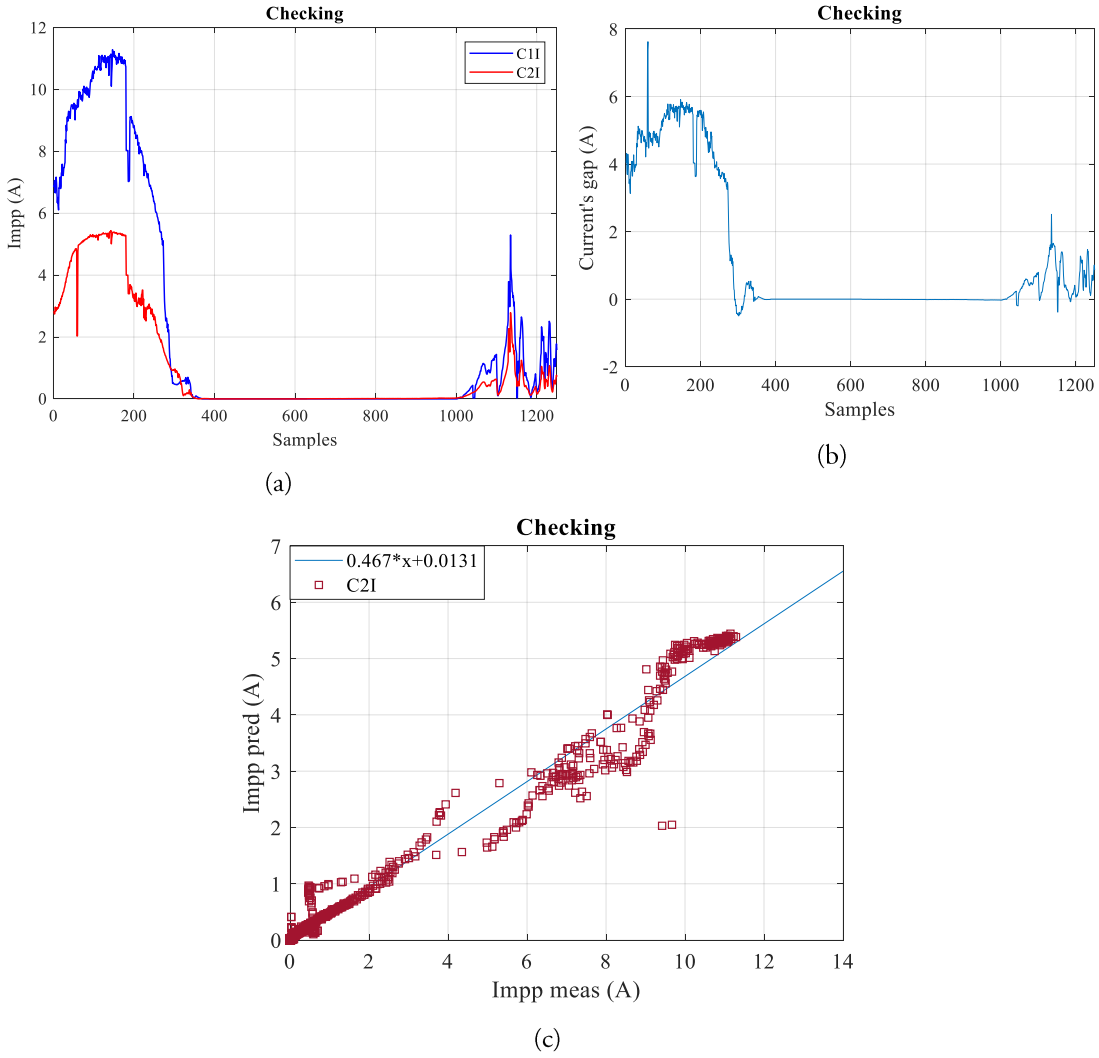

Fig. 26. Real healthy versus predicted open circuit branch in PV array of checking phase.

c. Testing

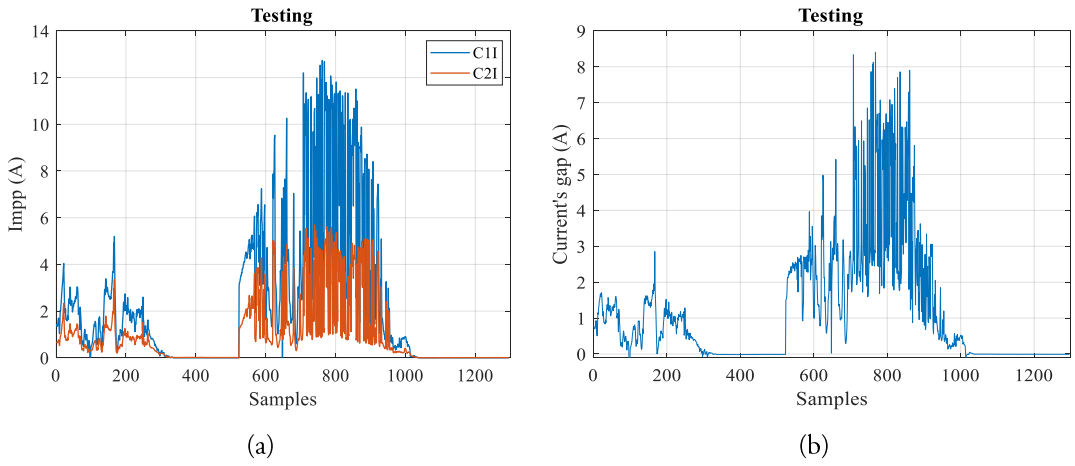

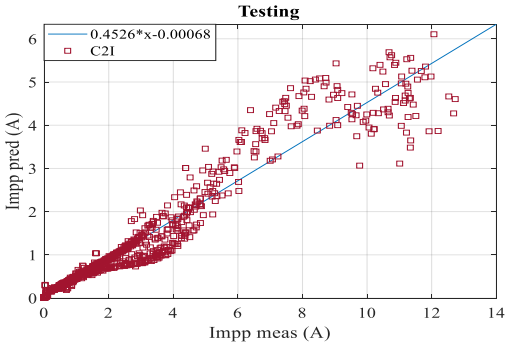

(c)

Fig. 27. Real healthy versus predicted open circuit branch in PV array of training phase.

5.8. Global faults Classification

5.8.1. Voltage

Fig. 28 shows the global voltage classification, in this case the healthy voltage is considered as concordance to identify and localize the deviation between predicted classes from CANFIS algorithm. For ground fault the voltage of PV array has around 93% fall, and for five PV modules short circuit fault the voltage decreases by 34%, around 12% lowering for two PV modules short circuit fault in PV array, while for two inversed by-pass diodes the voltage decreases by around 5% and it is too difficult to establish the identification of this class as most samples depict a misclassification with healthy voltage, and the deviation for healthy predicted voltage is around 99.9 %. In the goal to ensure an excellent level of precision and avoid the misclassification's voltage between classes, it should be inescapable to take in consideration only the part above 70V for healthy measured voltage with its corresponding faults in Vmpp predicted axe.

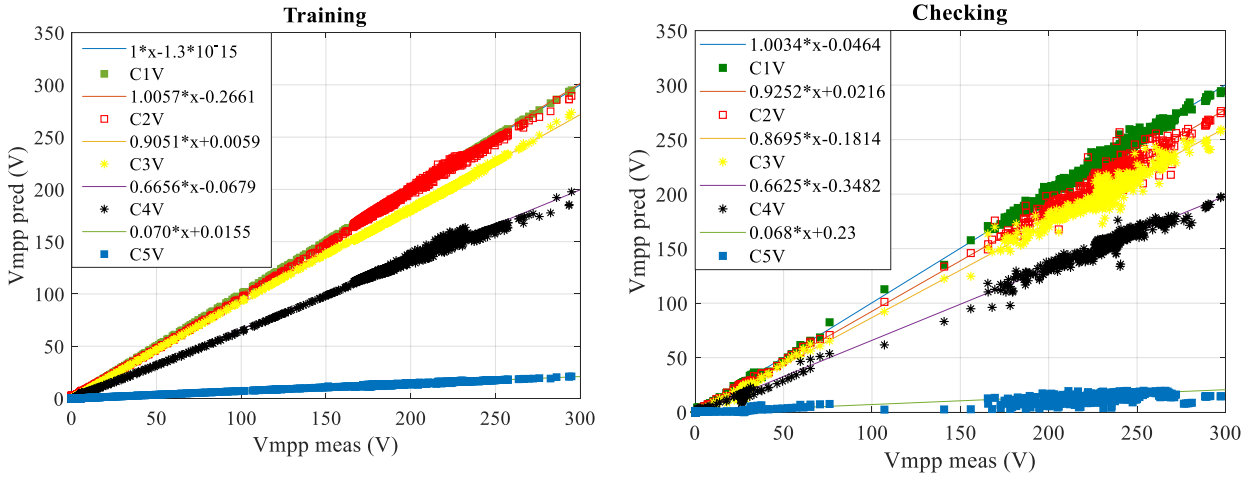

(a) (b)

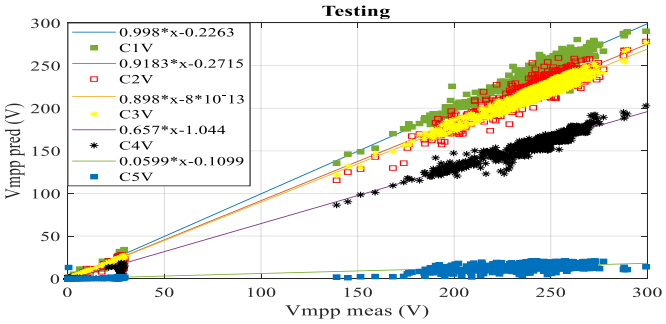

(c)

Fig. 28. CANFIS Global voltage classification, (a) training, (b) checking and (c) testing.

5.8.2. Current

Fig. 29 reveals the global current classification for training (a), checking (b) and testing (c) phases. That is uncomplicated to analyze the deviation between healthy measured data and both predicted cases from CANFIS (healthy and open circuit branch fault in PV array), the healthy current case has been taken as reference to be compare to the faulty case which is around 50% drop down in all phases (training, checking and testing). In order to guarantee the high quality of precision, it should be avoid to classify the current values under 3A for healthy measured current and its corresponding fault in Impp predicted axe.

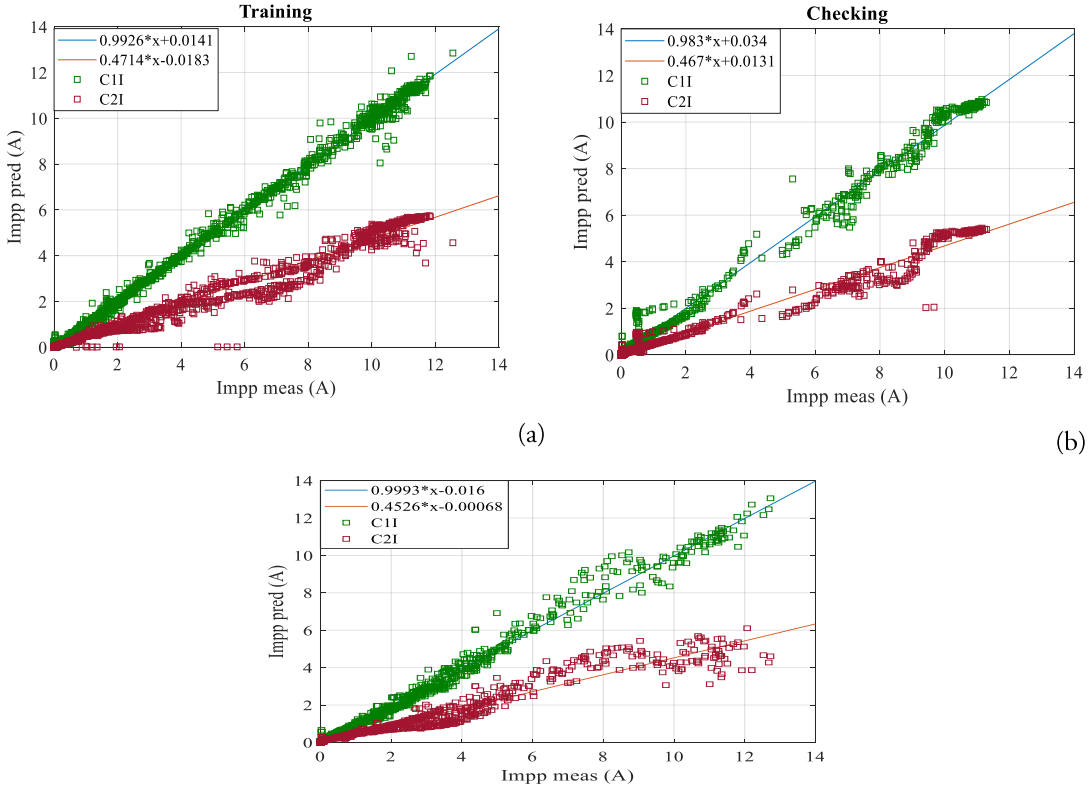

(a) (b)

(c)

Fig. 29. CANFIS Global current classification, (a) training, (b) checking and (c) testing.

6. Conclusion

The present paper brings a new approach in term of diagnosis, identification and recognition classes of small GCPV system by the employment of a hybrid Artificial Intelligence called co active neuro fuzzy logic (CANFIS). These process are necessary not solely to warrantee the stability, quality and reliability of the global PV system as well as best power generation but even to reduce human intervention with all the time that it takes. The novelty of the present study is to diagnose the most permanent faults be faced in PV system: open circuit PV branch, two PV modules short circuited, five PV modules short circuited, ground fault in addition to the two inversed by-pass diodes fault which was so difficult to diagnose where the solution has been successfully reached. The isolation and localization of fault diagnosis is based on electrical data (Vmpp, Impp) in two intelligent blocs separately. The First step is to test the performances of the proposed CANFIS algorithm by residual criteria citing: Mean square error (MSE), Root mean square error (RMSE), Mean absolute percentage error (MAPE), Mean absolute deviation (MAD) and coefficient of correlation (R2) which globally display an average of 4.65% and 0.99 for healthy electrical parameters. The second step is the isolation and the fault classification process which is considered as a fundamental part in this work by the employment of the scatter plot in linear percentage deviation between real healthy measured data and predicted data from CANFIS algorithm for all faults cases in addition to healthy case where it is clear to observe the lowering of different faults comparing to the healthy model with: 50% for open circuit branch in PV array, 93% for ground fault, 34% for five PV modules short circuit, 12% for two PV modules short circuit and 5% for two inversed by-pass diodes in PV array , knowing that all the classes treated in this approach contain their own signature under the notion of threshold in addition to the gap which changes from one class to another in order to avoid the problem of overlapping between classes, the CANFIS algorithm has succeeded in showing the accuracy of fault diagnosis for all studied classes of PV systems even for the fault relating to the bypass diode which at present has been remoted due to its difficult isolation.

Declaration of Competing Interest

The authors declare that they have no known competing financial interests or personal relationships that could have appeared to influence the work reported in this paper.

Acknowledgements

The authors acknowledge the financial support data from CDER plant in BP. 62 Bouzareah Observatory Road, 16340, Algiers (Algeria) as well as equipment support from Laboratory of electrical systems and remote control (SET Laboratory), Electronics Department, Blida 1 University, BP 270 Blida, Algeria.

References

[1] Silvestre S, Chouder A, Karatepe E. Automatic fault detection in grid connected PV systems. Sol. Energy 2013; 94: 119–27.

[2] Chine W, Mellit A, Pavan A M, Kalogirou S A. Fault detection method for grid-connected photovoltaic plants. Renew. Energy 2014 ; 66: 99–10.

[3] Platon R, Martel J, Woodruff N, Chau T.Y. Online fault detection in PV systems. IEEE Trans. Sustain. Energy 2015; 6 (4):1200–07.

[4] Drews A, de Keizer A.C, Beyer H.G, Lorenz E, Betcke J, van Sark W.G.J.H.M, Heydenreich W, Wiemken E, Stettler S, Toggweiler P, Bofinger S, Schneider M, Heilscher G, Heinemann D. Monitoring and remote failure detection of grid connected PV systems based on satellite observations. Sol. Energy 2007; 81: 548–64.

[5] Dhoke A, Sharma R, Kumar Saha T. An approach for fault detection and location in solar PV systems. Sol. Energy 2019; 194: 197-08.

[6] Garoudja E, Harrou F, Sun Y, Kara K, Chouder A, Silvestre S. Statistical fault detection in photovoltaic systems. Sol. Energy 2017; 150: 485-99.

[7] Chen Z, Chen Y, Wu L, Cheng S, Lin P. Deep residual network based fault detection and diagnosis of photovoltaic arrays using current-voltage curves and ambient conditions. Energy Convers. Manage 2019; 198: 111793.

[8] Solórzano J, Egido M.A. Automatic fault diagnosis in PV systems with distributed MPPT. Energy Convers. Manage 2013; 76: 925–34.

[9] Tina G.P, Cosentino F, Ventura F. Monitoring and Diagnostics of Photovoltaic Power Plants. World Renewable Energy Congress 2014, London, United Kingdom.

[10] Spataru S, Sera D, Kerekes T, Teodorescu R. Diagnostic method for photovoltaic systems based on light I–V measurements. Sol. Energy 2015; 119 : 29–44.

[11] Hare J, Shi X, Gupta S, Bazzi A. Fault diagnostics in smart micro-grids: a survey. Renew. Sustain. Energy Rev 2016; 60:1114–24.

[12] Silvestre S, daSilva M, Chouder A, Guasch D, Karatepe E. New procedure for fault detection in grid connected PV systems based on the evaluation of current and voltage indicators. Energy Convers. Manage 2014; 86:2 41–49.

[13] Tadj M, Benmouiza K, Cheknane A, Silvestre S. Improving the performance of PV systems by faults detection using GISTEL approach. Energy Convers. Manage 2014; 80:298–04.

[14] Siva Ramakrishna Madeti, S.N. Singh. Modeling of PV system based on experimental data for fault detection using kNN method. Sol. Energy 2018; 173: 139–151.

[15] Hussain M, Dhimish M, Titarenko S, Mather P. Artificial neural network based photovoltaic fault detection algorithm integrating two bi-directional input parameters. Renew. Energy 2020; 155: 1272–92.

[16] Belaout A, Krim F, Mellit A, Talbi B, Arabi A. Multiclass adaptive neuro-fuzzy classifier and feature selection techniques for photovoltaic array fault detection and classification. Renew. Energy 2018; 127: 548–58.

[17] Zhenghai L, Dazheng W, Liangliang T,Jinli R, Zhuming L. A Heuristic Diagnostic Method for a PV System: Triple-Layered Particle Swarm Optimization–Back-Propagation Neural Network, Energies 2017; 10:226.

[18] Garoudja E, Chouder A, Kara K, Silvestre S. An enhanced machine learning based approach for failures detection and diagnosis of PV systems. En Con Man 2017; 151: 496–13.

[19] Zhu H, Lub L, Yao J, Daia S, Hu Y. Fault diagnosis approach for photovoltaic arrays based on unsupervised sample clustering and probabilistic neural network model. Sol. Energy 2018; 176: 395–05.

[20] Kara Mostefa Khelil C, Amrouche B, Benyoucef AS, Kara K, Chouder A., New Intelligent Fault Diagnosis (IFD) Approach for grid-connected photovoltaic systems.,j.energy 2020; (211)118591.

[21] Kara Mostefa Khelil C, Amrouche B, Kara K, Chouder., The impact of the ANN's choice on PV systems diagnosis quality., En Con Man 2021; (240) 114278.

[22] Kara Mostefa Khelil C, Amrouche B, Kara K ., Fault detection and diagnosis of GCPV systems using Bayesian neural network., Journal of Physics: Conference 2022; (2208) 012019.

[23] Harrou F, Fillatre L, Nikiforov I. Anomaly detection/detectability for a linear model with a bounded nuisance parameter. Ann. Rev. Contr 2014; 38 (1):32–4.

[24] Chouder A, Silvestre S. Automatic supervision and fault detection of PV systems based on power losses analysis. Energy Convers. Manag 2010; 51: 1929-37.

[25] Gokmen N, Karatepe E, Celik B, Silvestre. Simple diagnostic approach for determining of faulted PV modules in string based PV arrays. Sol. Energy 2012; 86: 3364–77.

[26] Chouder A, Silvestre S. Analysis model of mismatch power losses in PV systems. Sol. Energy 2009; 131 (2):024504-4.

[27] Bastidas-Rodriguez J.D, Franco E, Petrone G, Ramos-Paja C.A, Spagnuolo G. Quantification of photovoltaic module degradation using model based indicators. Mathematics and Computers in Simulation 2017, 131:101-13.

[28] Takashima T, Yamaguchi J, Ishida M. Fault detection by signal response in PV module strings. In: Proceedings of the 33rd IEEE Photovoltaic Specialists Conference, 11–16 May 2008; 1–5.

[29] Johnson J, Kuszmaul S, Bower W, Schoenwald D. Using PV module and line frequency response data to create robust arc fault detectors. In: Proceedings of the 26th European Photovoltaic Solar Energy Conference and Exhibition, 05–09 September 2011, Hamburg, Germany; 3745–50.

[30] Takashima T, Yamaguchi J, Otani K, Oozeki T, Kato K, Ishida M. Experimental studies of fault location in PV module strings. Sol Energy Mater & Sol Cel 2009; 1079–82.

[31] Hachana O, Giuseppe Marco Tina, Hemsas K. PV array Fault Diagnostic Technique for BIPV Systems, Energy & Buildings 2016; (126) 263-74.

[32] Zhao Y, dePalma J, Mosesian J, Lyons R, Lehman B. Line–line fault analysis and protection challenges in solar photovoltaic arrays. IEEE Trans. Ind. Electron 2013; 60 (9):3784–95.

[33] Chen Z, Chen Y, Wu L, Cheng S , Lin. Deep residual network-based fault detection and diagnosis of photovoltaic arrays using current-voltage curves and ambient conditions. En Con Man 2019; (198) 111793.

[34] Li B, Delpha C, Diallo D, Migan-Dubois. Application of Artificial Neural Networks to photovoltaic fault detection and diagnosis: A review Ren & Sust Ener Rev 2021; (138) 110512.

[35] Madeti S R, Singh S N. Modeling of PV system based on experimental data for fault detection using kNN method Sol Energy 2018; (173) 139–51.

[36] Dhimish M, Holmes V, Mehrdadi B, Dales M. Comparing Mamdani Sugeno fuzzy logic and RBF ANN network for PV fault detection. Renew. Energy 2018; 117: 257–274.

[37] Dhimish M, Holmes V, Mehrdadi B, Dales M, Mather. Photovoltaic fault detection algorithm based on theoretical curves modelling and fuzzy classification system. J Energy 2017; (140) 276-90.

[38] Chine W, Mellit A, Lughi V, Malek A, Sulligoi G, Massi Pavan A. A novel fault diagnosis technique for photovoltaic systems based on artificial neural networks. Renew Energy 2016; 90: 501-512.

[39] Liao Z, Wang D, Tang L, Ren J, Liu Z. A Heuristic Diagnostic Method for a PV System: Triple-Layered Particle Swarm Optimization–Back-Propagation Neural Network. Energies 2017; 10 226.

[40] Belaout A, Krim F, Mellit A, Talbi B, Arabi A. Multiclass adaptive neuro-fuzzy classifier and feature selection techniques for photovoltaic array fault detection and classification. Renew. Energy 2018; 127: 548–58.

[41] Talei A, Chye Chua L H, Quek C. A novel application of a neuro-fuzzy computational technique in event-based rainfall–runoff modelling. Exp Syst with App 2010; 37: 7456-7468.

[42] Silva-Ramírez EL, Cabrera-Sánchez JF. Co-active neuro-fuzzy inference system model as single imputation approach for non-monotone pattern of missing data. Neural Comput & Applic 2021; 33: 8981–9004.

[43] Vieira J, Morgado Dias F, Mota A. Neuro-Fuzzy Systems: A Survey. 5th WSEAS NNA International conference on Neural Network and Applications: Udine, Italia, 25-27 March 2004.

[44] Lei Y. Intelligent Fault Diagnosis and Remaining Useful Life Prediction of Rotating Machinery. Xi'an Jiaotong University Press Co. Published by Elsevier 2017; Chap 3: p106.

[45] Tahmasebi P, Hezarkhani A. A hybrid neural networks-fuzzy logic-genetic algorithm for grade estimation. Comput & Geos 2012; 42: 18-27.

[46] Quej V .H, Almorox J, Arnaldo J .A., Saito L. ANFIS, SVM and ANN soft-computing techniques to estimate daily global solar radiation in a warm sub-humid environment. J of Atm and Sol–Ter Phys 2017; 155: 62-70.